[redacted]

[redacted]

Copy 217
RM L52I19a

NACA RM L52I19a

TECH LIBRARY KAFB, NM
0144451

[redacted]

NACA

RESEARCH MEMORANDUM

7368

THE EFFECTS OF A SMALL JET OF AIR EXHAUSTING FROM THE NOSE OF A BODY OF REVOLUTION IN SUPERSONIC FLOW

By Eugene S. Love

Langley Aeronautical Laboratory
Langley Field, Va.

RECEIPT SIGNATURE REQUIRED

CLASSIFIED DOCUMENT

This material contains information affecting the National Defense of the United States within the meaning of the espionage laws, Title 18, U.S.C., Secs. 793 and 794, the transmission or revelation of which in any manner to unauthorized person is prohibited by law.

NATIONAL ADVISORY COMMITTEE
FOR AERONAUTICS

WASHINGTON
November 12, 1952

[redacted]

[redacted]

Classification cancelled (or changed to Unclassified)

By Auth: Nasa Tech Pub Announcement #75

(OFFICER AUTHORIZED TO CHANGE)

By 21 Dec 54

(NAME OF OFFICER AUTHORIZED TO CHANGE) NK

14 Apr 61

DATE

TECH LIBRARY KAFB, NM
0144451

NATIONAL ADVISORY COMMITTEE FOR AERONAUTICS

RESEARCH MEMORANDUM

THE EFFECTS OF A SMALL JET OF AIR EXHAUSTING FROM THE NOSE OF A BODY OF REVOLUTION IN SUPERSONIC FLOW

By Eugene S. Love

SUMMARY

An investigation has been made at a Mach number of 1.62 to determine the effects of a small jet of air exhausting from the nose of an elliptical body of revolution upon boundary-layer transition and the viscous, pressure, and total drag of the forebody at three body stations. Schlieren photographs of the flow patterns in the vicinity of the body nose were also obtained. The tests were conducted at Reynolds numbers of 2.13×10^6 and 7.66×10^6, based on body length. The maximum range of thrust coefficients for the small jet was from 0 to about -0.085.

At the lower test Reynolds number, for which the boundary layer was laminar over the entire body in the jet-off condition, a very small flow from the jet moved the point of transition forward to the vicinity of the 20-percent-body station. As the jet flow was increased, the transition point moved abruptly to the nose at a thrust coefficient of about -0.013. The jet caused large reductions in forebody pressure drag regardless of the type of boundary layer. At the higher test Reynolds number for which the boundary layer was largely turbulent in the jet-off condition the total drag, including skin friction, was reduced somewhat by the action of the jet.

Although the forward-exhausting small jet was found to have the above favorable effects upon the drag, these findings are not believed too important since the question arises as to the benefits of the same small jet exhausting from the rear of the body in the conventional manner. No attempt was made to establish geometric optimums in the present investigation, yet, from a general consideration of the benefits indicated by the present results and the phenomena known to occur in the vicinity of rearward-exhausting jets, the benefits of a small jet exhausting rearward would appear to exceed those of the same small jet exhausting forward, particularly so when the flow over the body is laminar in the jet-off condition.

HAFB-2-196

INTRODUCTION

As a result of recent experimental and theoretical investigations into the shock—boundary-layer phenomena associated with blunt-nosed bodies (see refs. 1, 2, and 3) some interest has been centered upon what might be achieved by exhausting a small jet of air near the stagnation point of a blunt-nosed body or of a wing with rounded leading edge. A limited investigation conducted in the Langley 9-inch supersonic tunnel has shown what effects a small jet exhausting from the nose of an elliptical body of revolution may have upon boundary-layer transition and the skin-friction and pressure drag of the forebody at a Mach number of 1.62. This investigation was undertaken primarily to give a clearer understanding of the pressure-drag variations measured in a related project conducted by the Flight Research Division (ref. 3) and to determine what over-all drag benefits, if any, might be realized. While present interest is centered on the effects of a small jet upon the skin-friction drag and boundary-layer transition, all the results of the investigation are presented herein since they show the relation between the surface pressures and the viscous scavenging phenomena created by the jet.

The Reynolds numbers for the tests were 2.13×10^6 and 7.66×10^6 based on body length, the former giving laminar flow over the entire body and the latter giving turbulent flow over most of the body (small jet inoperative). The range of thrust coefficients for the small jet was from 0 to about -0.085.

SYMBOLS

A_j area of jet exit

A_{max} maximum cross-sectional area of body

β temperature recovery factor

C_T thrust coefficient, $\dfrac{T}{q_o A_{max}}$

$\Delta P = P_{(jet\ on)} - P_{(jet\ off)}$

θ_c compressible momentum thickness

$\delta_c{}^*$ compressible displacement thickness

R	Reynolds number
δ	boundary-layer thickness
$\Delta C_{D_T} = \left(\Delta C_{D_p} - C_T\right) + \Delta C_{D_f}$	
$\Delta C_{D_f} = C_{D_{f(\text{jet on})}} - C_{D_{f(\text{jet off})}}$	
C_{D_p}	forebody pressure drag coefficient
ΔC_{D_p}	change in C_{D_p} caused by jet
C_{D_f}	skin-friction drag coefficient
C_{D_T}	total drag coefficient
L	total length of body
M	Mach number
p_l	local static pressure
p_o	stream static pressure
q_o	stream dynamic pressure
P	pressure coefficient, $\frac{p_l - p_o}{q_o}$
p_{o_j}	stagnation pressure of jet
q_j	dynamic pressure of jet
r	radius of model
ρ	density
T	thrust
U	velocity
u	velocity within boundary layer

x distance from nose of body measured along body center line

y distance normal to body center line

Subscript:

δ value just outside boundary layer

APPARATUS

Wind Tunnel

The Langley 9-inch supersonic tunnel is a continuous-operation, closed-circuit type in which the pressure, temperature, and humidity of the enclosed air can be regulated. Different test Mach numbers are provided by interchangeable nozzle blocks which form test sections approximately 9 inches square. Eleven fine-mesh turbulence-damping screens are installed in the relatively large area settling chamber ahead of the supersonic nozzle. A schlieren optical system is provided for flow observations.

Model

A drawing of the model giving the orifice locations and the details of the small jet are shown in figure 1. The elliptical body had a fineness ratio of 6 and its shape equation was

$$\left(\frac{x - 3}{3}\right)^2 + (2y)^2 = 1 \tag{1}$$

As shown, the hollow sting support served as the air conduit for the small jet. The internal diameter of the small length of tube which formed the jet exit was 0.030 inch. A stagnation-pressure lead was vented to the inside of the hollow sting support near the point within the model where the support began its initial reduction in cross-sectional area (see fig. 1). This lead tube was conducted out the rear of the model, together with the orifice lead tubes, by means of an access hole parallel with and adjacent to the sting support. The lead tubes were soldered and faired compactly to the sting support.

The model was made of steel and its surface was highly polished. The machined ordinates were within 0.001 inch of the specified values. Measurements of surface roughness showed that, excluding the region near the nose, the model had a roughness of 5 to 8 rms microinches. Close to

the nose the roughness increased considerably, and deviations of as much as 300 rms microinches were measured. These deviations appeared to be localized tool troughs rather than roughness in the usual sense. In addition, the necessary close spacing of the orifices near the nose probably added to the surface imperfections in this region and along the meridian in which the orifices were located.

Boundary-Layer Survey Apparatus

A drawing of the boundary-layer survey apparatus employed in measuring the profiles at three stations along the body is shown in figure 2. The locations of these three stations with respect to the body nose are indicated in figure 1. Basically, the survey apparatus is a single-probe micrometric traversing system mounted on a plate which replaces one of the tunnel windows. Dimensions of the head of the total-pressure probe obtained by microscopic measurements are presented in figure 2(b). A low-voltage electrical contact system was used to detect the breakaway of the probe from the model surface.

TESTS AND PROCEDURE

All tests were conducted at a Mach number of 1.62 and at zero pitch and yaw with respect to the tunnel side walls and center line, respectively. The air for operating the small jet was obtained from the dry-air storage tanks employed in tunnel operation for which the maximum storage pressure is 500 pounds per square inch. Jet operation was limited, therefore, to a jet stagnation pressure range from approximately 0 to 450 pounds per square inch. The jet stagnation pressure was controlled by means of a manual gate valve and recorded on a dial pressure gage. For the above pressure range, tests were conducted at Reynolds numbers, based on body length, of 2.13×10^6 and 7.66×10^6 which permitted maximum thrust coefficients of approximately -0.085 and -0.023, respectively (negative by convention). For each Reynolds number and at varying thrust coefficients, the tests included: (1) measurements of the pressures over the body, (2) schlieren photographs and shadowgraphs of the phenomena, and (3) boundary-layer surveys at body stations of $\frac{x}{L} = 0.150$, 0.483, and 0.767. The pressure measurements over the body were not made beyond $\frac{x}{L} = 0.767$, since the region is being approached where sting-interference effects would influence the pressures. Throughout the tests the dew point was kept sufficiently low to insure that the effects from condensation were negligible.

REDUCTION OF DATA

For calculating the thrust of the jet, the assumptions were made that the losses in the length of tube from the point at which the stagnation pressure was measured to the exit were negligible and that the Mach number at the jet exit was unity. With these assumptions the thrust of the jet is given by

$$T = A_j\left(2q_j + 0.5283p_{o_j} - p_o\right) \tag{2}$$

The error introduced by using equation (2) for the few cases in which the Mach number at the exit is less than 1 is believed to be small.

For calculating the skin-friction drag coefficients the values of θ_c and $\delta_c{}^*$ were determined as in reference 4 from

$$\theta_c = \frac{1}{M_\delta{}^2}\int_0^\delta \left[MM_\delta\left(\frac{5 + \beta M^2}{5 + \beta M_\delta{}^2}\right)^{1/2} - M^2\right]dy \tag{3}$$

and

$$\delta_c{}^* = \int_0^\delta \left[1 - \frac{M}{M_\delta}\left(\frac{5 + \beta M^2}{5 + \beta M_\delta{}^2}\right)^{1/2}\right]dy \tag{4}$$

and applied to the expression

$$C_{D_f} = \frac{2\pi}{qA_{max}}\left[r\rho_\delta U_\delta{}^2\theta_c + \int_0^x \rho_\delta U_\delta r\delta_c{}^* \frac{dU_\delta}{dx}\,dx + \rho_\delta U_\delta{}^2\int_0^\delta\left(\frac{\rho u}{\rho_\delta U_\delta} - \frac{\rho u^2}{\rho_\delta U_\delta{}^2}\right)y\,dy\right] \tag{5}$$

which does not include a second-order term in $\delta_c{}^*$ since its contribution to C_{D_f} is less than 1 percent. The results of reference 4 have shown this expression to be sufficiently accurate for evaluating the skin-friction drag of slender parabolic bodies. In the present calculations

the variation of δ_c^* with x was determined from a curve faired through the measured values at the different body stations and by assuming that both δ_c^* and θ_c became zero at the nose for all thrust coefficients. The error introduced by such an assumption is believed to be small except at the higher thrust coefficients where the mass flow of the jet becomes appreciable in relation to the mass flow within the boundary layer. In equations (3) and (4), temperature recovery factors of 0.88 and 1 were used when the boundary layer was known to be laminar and turbulent, respectively, at the particular station under investigation. (See ref. 4.)

PRECISION

During the tests the model was maintained at zero pitch within $\pm 0.1^\circ$ with respect to the tunnel side walls and at zero yaw within $\pm 0.07^\circ$ with respect to the tunnel center line. Past measurements of the flow angularity in the tunnel test section have shown negligible deviations. The estimated accuracies of the test variables and the various coefficients are as follows:

Mach number, M	± 0.01
Reynolds number, R	$\pm 0.04 \times 10^6$
Pressure coefficient, P	± 0.002
Forebody pressure drag coefficient, C_{D_p}	± 0.002
Thrust coefficient, C_T	± 0.0002

Investigations of the total-pressure probe used in the boundary-layer surveys have shown that, for ratios of probe height to boundary-layer thickness of 1/3 or less, the probe has no measurable effect upon the condition or thickness of the boundary layer and that it experiences no measurable deflections in traversing the boundary layer at a given Reynolds number of the flow. However, in the present tests the probe height was considerably greater than 1/3 the boundary-layer thickness for the laminar profiles at $\frac{x}{L} = 0.150$ and 0.483 for $R = 2.13 \times 10^6$, and for the profiles at $\frac{x}{L} = 0.150$ for $R = 7.66 \times 10^6$. The effect of the probe for these conditions is not known; therefore, while the profile shapes for these conditions may be indicative of the type of boundary layer, the skin-friction coefficients computed from these profiles should be accepted with considerable caution.

An indication of the reliability of skin-friction values determined from surveys with this probe when the probe height is 1/3 the boundary-layer thickness, or less, may be seen in reference 4 where good agreement

was shown between the values computed from the profiles and those obtained from force and pressure measurements. In the present tests probe position could be measured within ±250 microinches and repeated within an estimated ±500 microinches.

RESULTS AND DISCUSSION

Effects of jet upon body pressures.- The experimental pressure distributions over the forebody are presented in figure 3(a) for a Reynolds number of 2.13×10^6 and in figure 3(b) for a Reynolds number of 7.66×10^6. The effect of increasing C_T (negatively) in decreasing the body pressures near the nose is clearly shown. Most of this effect is confined to the forward 5 percent of the body. Figure 4, which presents the change in local pressure coefficient with C_T for the first four orifices, gives a further indication of the localization of this beneficial reduction in body pressures and shows that all the orifices initially experience an increase in pressure. Also indicated is the almost negligible effect of increase in free-stream Reynolds number upon the change in these body pressures.

As shown by the curves of figure 3 the peak pressures move rearward with increasing thrust coefficient. The locations of these peak pressures are presented in figure 5 as a function of thrust coefficient. (These locations were taken from enlarged curves employed in evaluating the pressure drag.) Also entered in figure 5 are curves which show the thrust coefficient for maximum pressure and the thrust coefficient ($C_T \neq 0$) for which $\Delta P = 0$ at a given body station, as established by the data of figure 4. Comparisons of these curves indicate that a body station experiences its maximum pressure at a thrust coefficient lower than that for which the pressure peak would occur at the station and that the peak pressure approaches closely the pressure at that station for $C_T = 0$ (see insert fig. 5).

Correlation of pressure variations with observed phenomena.- Some insight into the variations exhibited by the curve of figure 5 defined by the peak-pressure locations is gained from the shadowgraphs and schlieren photographs of figures 6 and 7 and the sketches of the phenomena in figure 8. The phenomena in the vicinity of the nose appear to be independent of the Reynolds number of the flow; therefore, no differentiation is made in this regard in the following discussion.

At $C_T = 0$ (jet off) a detached bow wave exists ahead of the nose. As the jet begins to flow, a near-conical shock is formed which protrudes ahead of the location of the original bow wave and is followed by a second

shock necessary to turn the flow in a direction determined by the effects of the body upon the inclination of the boundary of the turbulent spillage from the jet. The near-conical and the secondary shock join a short distance away from the body to form the single bow wave. As C_T increases, and the jet remains subsonic, this point of juncture moves outward and the tip of the near-conical shock moves forward. These general characteristics of the phenomena continue until the jet first becomes supersonic. When this occurs the near-conical shock immediately jumps rearward, losing its near-conical shape and taking the rounded shape of a bow wave. This abrupt change was observed for both increasing and decreasing thrust coefficient. The sketch in figure 8(c) is typical of the new form of the jet-shock phenomena.

Based upon the assumption that the static pressure acting against the jet exit is the stagnation pressure behind a normal shock at $M = 1.62$, the value of C_T for initial supersonic flow was computed to be approximately -0.0042. The two schlieren photographs of figure 7(a) at $C_T = -0.0051$ show that this value corresponds to the experimental start of supersonic flow. The difference between the actual and calculated values of C_T is probably due to the inadequacy of the above assumption and the losses within the small jet tube. The experimental results of figure 5 show that the peak pressure suddenly moves back on the body at $C_T = -0.0054$. The explanation for this sudden rearward movement may be seen in the sketches of figure 8 and by examination of figures 6 and 7. As long as the jet remains subsonic, the secondary shock remains just ahead of the body nose. When the jet becomes supersonic and the near-conical shock collapses to a rounded shape, the secondary shock comes in contact with the body nose, and the point from which it stems is determined by the abrupt change in flow direction at the intersection of the well-defined (as compared with the subsonic jet) boundary of the jet spillage and the body surface. The sudden rearward movement in the pressure peak, therefore, correlates with the rearward movement of the secondary shock to a position of contact with the body nose, and the existence of a pressure peak correlates with the rise in pressure through the secondary shock.

Once the jet is supersonic, there is apparently no change in the pressure-peak location until C_T reaches a value of about -0.013. Figures 6 and 7 show that within this range the secondary shock appears to remain stationary, its base being almost coincident with the nose of the body. Beyond a value -0.013 there is a rearward movement of the secondary shock and the boundary of the jet spillage appears to become more turbulent and less well defined. Near $C_T = -0.02$, the jet spillage loses its tendency to turn in toward the body and streams rearward in a highly turbulent manner, intersecting the body less acutely and thereby causing a weaker secondary shock. Between $C_T = -0.013$ and -0.02, figure 5 shows

the pressure peak to move rearward in a manner similar to the secondary shock movement. Beyond $C_T = -0.02$, the rearward movement of the pressure peak with increasing C_T becomes essentially linear, falling off slightly at the highest thrust coefficients. In like manner, figures 6 and 7 show that once the phenomena is such as sketched in figure 8(d), there is a steady rearward movement of the secondary shock with increasing C_T. In this range the expansion bulb formed by the exhausting jet continues to grow, and its increasing diameter causes the turbulent jet spillage to intersect the body farther and farther rearward thereby causing weaker secondary shocks which tend to "lambda" into the turbulent spillage. At the same time, the growth of the expansion bulb also causes a stronger bow wave which at $C_T = -0.0852$ appears stronger than the original bow wave at $C_T = 0$.

Although a distinct correlation between the movement of the secondary shock and the movement of the peak pressure has been shown, all of the pressure rise may not be a result of the secondary shock alone. The phenomena as sketched in figure 9 are believed to represent more accurately how the peak pressure is realized, as well as the reduction in pressures ahead of the peak. The induction effects at the boundary of the jet expansion bulb cause a rotation of the flow as shown in the region between the expansion-bulb boundary and the limits of the turbulent spillage. To the left of some point P this rotation tends to scavenge the air away from the body surface, thereby reducing the pressures. At the point P the flow is normal to the surface and creates a stagnation point insofar as the spillage and turbulent interchange is concerned. To the right of point P the flow is deflected by the surface and continued downstream. Thus, a stagnation point P may be determined without the presence of the secondary shock. However, as the experimental results show, the turbulent spillage meets the body surface at some finite angle and the secondary shock arises. The presence of this shock and the resulting pressure increase would very likely cause the stagnation point P to be nearer the body nose than would be the case in its absence.

From the above reasoning, the peak pressure appears to be created by a combination of the presence of the secondary shock and a stagnation of the circulation within the turbulent spillage. However, while such seems likely, it does not seem necessarily true that the peak pressure would occur exactly at P. The increase in pressure caused by the shock might be greater than the stagnation potential of the circulating turbulent spillage, which is undoubtedly experiencing large energy losses in the form of viscous scavenging and turbulent exchange, and, if such were the case, the peak pressure might occur between P and the base of the secondary shock.

Figure 10 presents results at $M = 0$ and at atmospheric pressure of the variation of the pressures at the first two orifices with increasing

C_T. (In computing C_T, the value of q_o for $R = 2.13 \times 10^6$ was used in order that relative comparisons may be made between the observed phenomena at $M = 0$ and $M = 1.62$.) The decrease in pressure shown for these orifices indicates the existence of viscous scavenging. The shadowgraphs show the formation of the jet expansion bulb in the absence of impinging flow.

The values of forebody pressure drag obtained from the experimental pressure distributions of figure 3 are presented in figure 11 for the two Reynolds numbers and for the portions of the forebody ahead of the three stations at which boundary-layer surveys were made. The effect of the jet in decreasing the forebody pressure drag is appreciable. At $C_T = -0.0852$ the reduction is more than one-half of the pressure drag at $C_T = 0$. The absolute amount of this reduction is shown in figure 12. Here again the negligible effect of Reynolds number is shown as well as the indicated confinement of the reduction to the region of the body near the nose. In figure 13 the detrimental increase in drag due to the thrust of the jet has been subtracted from the beneficial decrease in pressure drag. The resultant values represent the over-all drag change, exclusive of changes in skin friction, from the nose to the three body stations. Initially there is a very slight increase followed by a rapid decrease. A maximum reduction in drag coefficient of approximately -0.029 is realized at a value of C_T of about -0.05. At larger values of C_T the drag reduction shows a general decrease.

Effects of jet upon boundary-layer transition and skin friction.- Boundary-layer profiles measured at the three body stations are presented in terms of local Mach number in figures 14 and 15 for the two Reynolds numbers. Figure 16 presents the location of the transition point on the body as a function of thrust coefficient. These locations were determined where possible from enlarged schlieren photographs as in references 4 and 5 in which good agreement was shown for the positions thus indicated and those determined by boundary-layer surveys.

Though it is possible that all the energy of the jet flow may not be dissipated in completing the approximately 180° turn forced upon it by the impinging free stream, if any such energy remains in the form of velocities within the boundary layer that are higher than would be the case at $C_T = 0$, then they are not sufficiently localized to be detected in the profiles of figures 14 and 15. In reducing the profile data, the total pressure at the edge of the boundary layer was noted to be rather consistently about 1.08 times the total-pressure recovery behind a normal shock at $M = 1.62$. Other than the direct indication of losses less than normal shock losses, the significance of the 1.08 factor is not apparent.

At the lower Reynolds number $\left(R = 2.13 \times 10^6\right)$, for which laminar flow was observed over the entire body in the jet-off condition, the most

significant effect of the jet is to cause transition to occur well forward on the body. This is indicated in figure 16 where the transition point is shown to move forward rapidly with increasing values of C_T less than about -0.003; with further increase in C_T the transition point moves forward slowly. Comparison of the profiles of figure 14 with figure 16 appears to indicate a general correlation between the profile shape and the location of the transition point. At $\frac{x}{L} = 0.150$ extrapolation to the curve of figure 16 indicates that the profiles should be laminar for $C_T = 0$ to about -0.013 and turbulent beyond $C_T = -0.013$. Similarly, at $\frac{x}{L} = 0.483$ the profiles should be turbulent beyond $C_T = -0.0022$; and at $\frac{x}{L} = 0.767$ the profiles should be turbulent beyond $C_T = -0.001$. The profiles of figures 14(a), (b), and (c) substantiate these indications. In like manner for $R = 7.66 \times 10^6$, at $\frac{x}{L} = 0.150$ extrapolation to the curve of figure 16 shows the profiles should be turbulent beyond $C_T \approx -0.01$; at $\frac{x}{L} = 0.483$ and 0.767 all profiles should be turbulent. Again, the profiles of figure 15 tend to substantiate these indications with the possible exception of figure 15(a) for $\frac{x}{L} = 0.150$ where the large ratio of probe height to boundary-layer thickness probably masks any appreciable change in profile shape.

In the previous discussions of the jet phenomena the observation was made, on the basis of the rather strong indications of figures 6 and 7, that the spillage from the jet was turbulent. The enlarged photographs used to obtain the data for figure 16 seemed to confirm this but also indicated that the turbulence of the spillage tended to become damped in nearing the body surface to the extent that at some point on the body at or very near the nose the boundary layer becomes laminar. This point, or the point at which the turbulent spillage ceases to mask the laminar boundary layer, appears to move slightly rearward with increasing thrust coefficient when the jet is both subsonic and supersonic provided C_T does not exceed approximately -0.013. When the jet is supersonic the turbulence of the spillage seems to be lessened considerably. From its initial point, the laminar run continues for a short distance until the point of natural transition is reached. Figure 3 shows that in this region of laminar flow there is a highly favorable pressure gradient. With increasing thrust coefficient, this region of laminar flow tends to become smaller since, as shown in figure 16, the point of natural transition moves forward, probably because of the increased turbulence level of the flow wetting the body. Thus, the laminar region continues to decrease until at a thrust coefficient in the vicinity of -0.013 $\left(\text{for } R = 2.13 \times 10^6\right)$ the small remaining laminar

region is suddenly eliminated. In the discussion of the phenomena of figures 6 and 7, the secondary shock was shown to exhibit no appreciable rearward movement onto the body surface until a value of $C_T = -0.013$ was exceeded. The sudden elimination of the small remaining laminar region near this value of C_T appears, therefore, to be the result of shock—boundary-layer interaction at the base of the secondary shock causing transition to turbulent flow.

In view of the effect of the jet in creating greater regions of turbulent flow over the body, particularly at $R = 2.13 \times 10^6$, the previously presented over-all drag reduction $\left(\Delta C_{D_p} - C_T\right)$ exclusive of skin friction would be somewhat offset by the rise in skin friction. Skin-friction drag coefficients calculated for several conditions are presented in the table to follow. These values are subject to the inadequacies previously discussed in the section covering precision:

Station, $\frac{x}{L}$	$R = 2.13 \times 10^6$		$R = 7.66 \times 10^6$	
	C_T	C_{D_f}	C_T	C_{D_f}
0.150	0	0.0054	0	0.0060
.483	0	.0150	0	.0255
.767	0	.0194	0	.0470
.150	-.0027	.0081	-.0019	.0088
.483	-.0027	.0287	-.0019	.0252
.767	-.0027	.0503	-.0019	.0487
.150	-.0758	.0195	-.0224	.0084
.483	-.0758	.0360	-.0224	.0313
.767	-.0758	.0734	-.0224	.0588

At $C_T = 0$, the low values of skin-friction drag for the lower Reynolds number correspond to laminar flow. Though the change in C_{D_f} at the forward station at $C_T = 0$ as a result of increasing Reynolds number opposes what might be expected, the indicated difference is within the accuracy of the calculations, and the values of C_{D_f} may be taken as having the same order of magnitude and corresponding to laminar flow. The higher values of C_{D_f} at the middle and rear stations at $C_T = 0$ for the higher Reynolds number correspond to turbulent flow. At $R = 2.13 \times 10^6$ and $C_T = -0.0027$ the general agreement between the values of C_{D_f} at the middle and rear stations with the values at the corresponding stations for

$C_T = 0$ and $R = 7.66 \times 10^6$ shows that at the lowest thrust coefficients the effect of the jet is merely to trigger turbulence at these stations. This effect is further substantiated by a comparison of the values at $C_T = 0$ and -0.0019 at $R = 7.66 \times 10^6$ at the middle and rear stations. In view of the above, the general agreement shown at the lowest thrust coefficients between the values of C_{D_f} for both Reynolds numbers would be expected. The effect of high thrust coefficients is to increase C_{D_f}, particularly at the rear station.

Jet effects upon total drag (exclusive of base drag).- The effect of the jet in increasing skin-friction drag ΔC_{D_f} has been added to the previously presented values of $\left(\Delta C_{D_p} - C_T\right)$ to obtain the change in total drag ΔC_{D_T}. The resulting values of ΔC_{D_T} are tabulated below:

Station, $\frac{x}{L}$	$R = 2.13 \times 10^6$		$R = 7.66 \times 10^6$	
	C_T	ΔC_{D_T}	C_T	ΔC_{D_T}
0.150	-0.0027	-0.0027	-0.0019	0.0028
.483	-.0027	.0093	-.0019	0
.767	-.0027	.0263	-.0019	.0017
.150	-.0758	-.0054	-.0224	-.0188
.483	-.0758	.0015	-.0224	-.0154
.767	-.0758	.0340	-.0224	-.0106

The values of ΔC_{D_T}, together with the results of figure 13, indicate that, when the flow over the body is laminar at $C_T = 0$, the effect of the jet upon the total drag is predominantly unfavorable because of the increase in skin friction resulting from the large regions of turbulent boundary layer created by the jet. When the flow over most of the body is turbulent at $C_T = 0$, the jet can cause appreciable reduction in total drag.

CONCLUDING REMARKS

The results of the present investigation at a Mach number of 1.62 have shown what effects a small jet of air exhausting from the stagnation point of an elliptical body of revolution may have upon boundary-layer transition and the viscous, pressure, and total drag of the forebody at

three body stations for Reynolds numbers of 2.13×10^6 and 7.66×10^6, based on body length.

At the lower test Reynolds number, for which the boundary layer was laminar over the entire body in the jet-off condition, a very small flow from the jet moved the point of transition forward to the vicinity of the 20-percent-body station. As the jet flow was increased, the transition point moved abruptly to the nose at a thrust coefficient of about -0.013. The jet caused large reductions in forebody pressure drag regardless of the type of boundary layer. At the higher test Reynolds number for which the boundary layer was largely turbulent in the jet-off condition the total drag, including skin friction, was reduced somewhat by the action of the jet.

Although the forward-exhausting small jet was found to have the above favorable effects upon the drag, these findings are not believed too important since the question arises as to the benefits of the same small jet exhausting from the rear of the body in the conventional manner. No attempt was made to establish geometric optimums in the present investigation, yet, from a general consideration of the benefits indicated by the present results and the phenomena known to occur in the vicinity of rearward-exhausting jets, the benefits of a small jet exhausting rearward would appear to exceed those of the same small jet exhausting forward, particularly so when the flow over the body is laminar in the jet-off condition.

Langley Aeronautical Laboratory,
National Advisory Committee for Aeronautics,
Langley Field, Va.

REFERENCES

1. Jones, Jim J.: Flow Separation From Rods Ahead of Blunt Noses at Mach Number 2.72. NACA RM L52E05a, 1952.

2. Moeckel, Wolfgang E.: Flow Separation Ahead of a Blunt Axially Symmetric Body at Mach Numbers 1.76 to 2.10. NACA RM E51I25, 1951.

3. Lopatoff, Mitchell: Wing-Flow Study of a Pressure-Drag Reduction at Transonic Speed by Projecting a Jet of Air From the Nose of a Prolate Spheroid of Fineness Ratio 6. NACA RM L51E09, 1951.

4. Love, Eugene S., Coletti, Donald E., and Bromm, August F., Jr.: Investigation of the Variation With Reynolds Number of the Base, Wave, and Skin-Friction Drag of a Parabolic Body of Revolution (NACA RM-10) at Mach Numbers of 1.62, 1.93, and 2.41 in the Langley 9-Inch Supersonic Tunnel. NACA RM L52H21, 1952.

5. Jack, John R., and Burgess, Warren C.: Aerodynamics of Slender Bodies at Mach Number of 3.12 and Reynolds Numbers From 2×10^6 to 15×10^6. I - Body of Revolution With Near-Parabolic Forebody and Cylindrical Afterbody. NACA RM E51H13, 1951.

CONFIDENTIAL

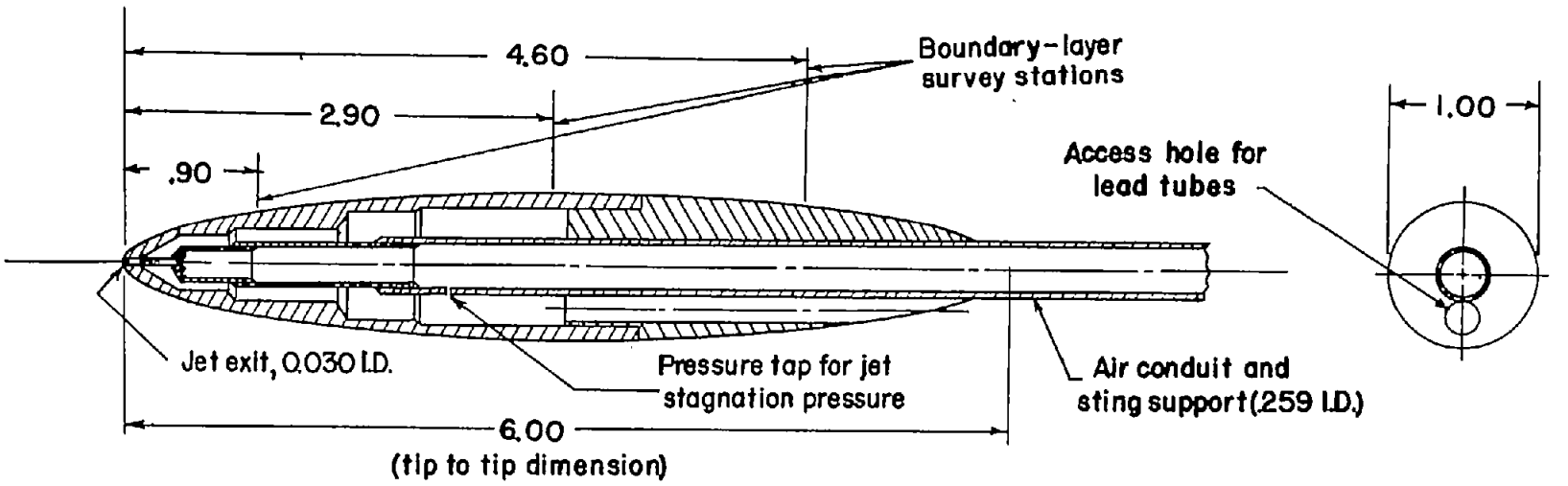

Orfice locations, X	
0.050	1.200
0.100	1.400
0.150	1.800
0.200	2.100
0.300	2.400
0.400	2.700
0.500	2.900
0.600	4.050
0.800	4.600
1.000	

Figure 1.- Drawing of model. All dimensions are in inches.

CONFIDENTIAL

CONFIDENTIAL

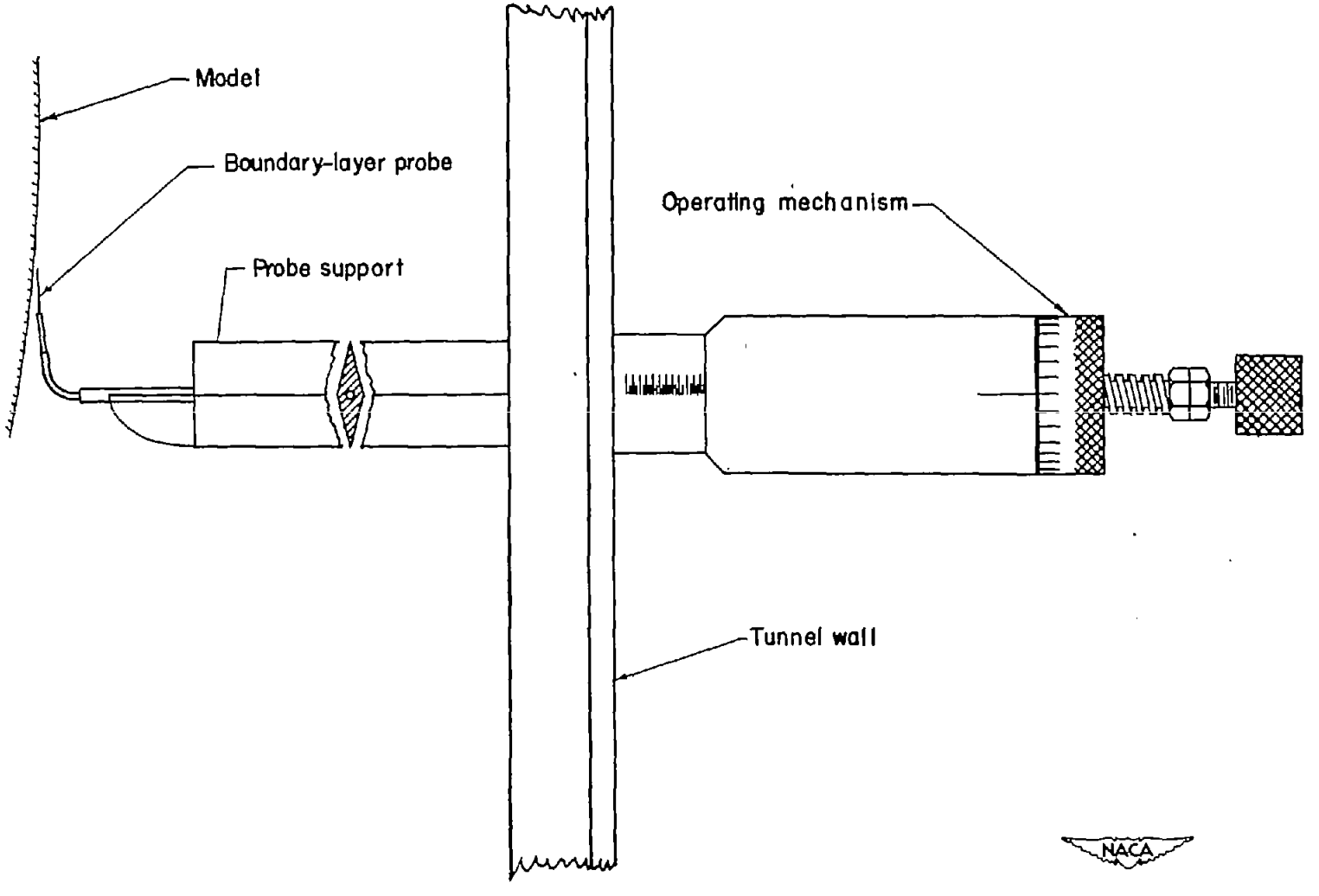

(a) Support and operating mechanism.

Figure 2.- Boundary-layer survey apparatus.

CONFIDENTIAL

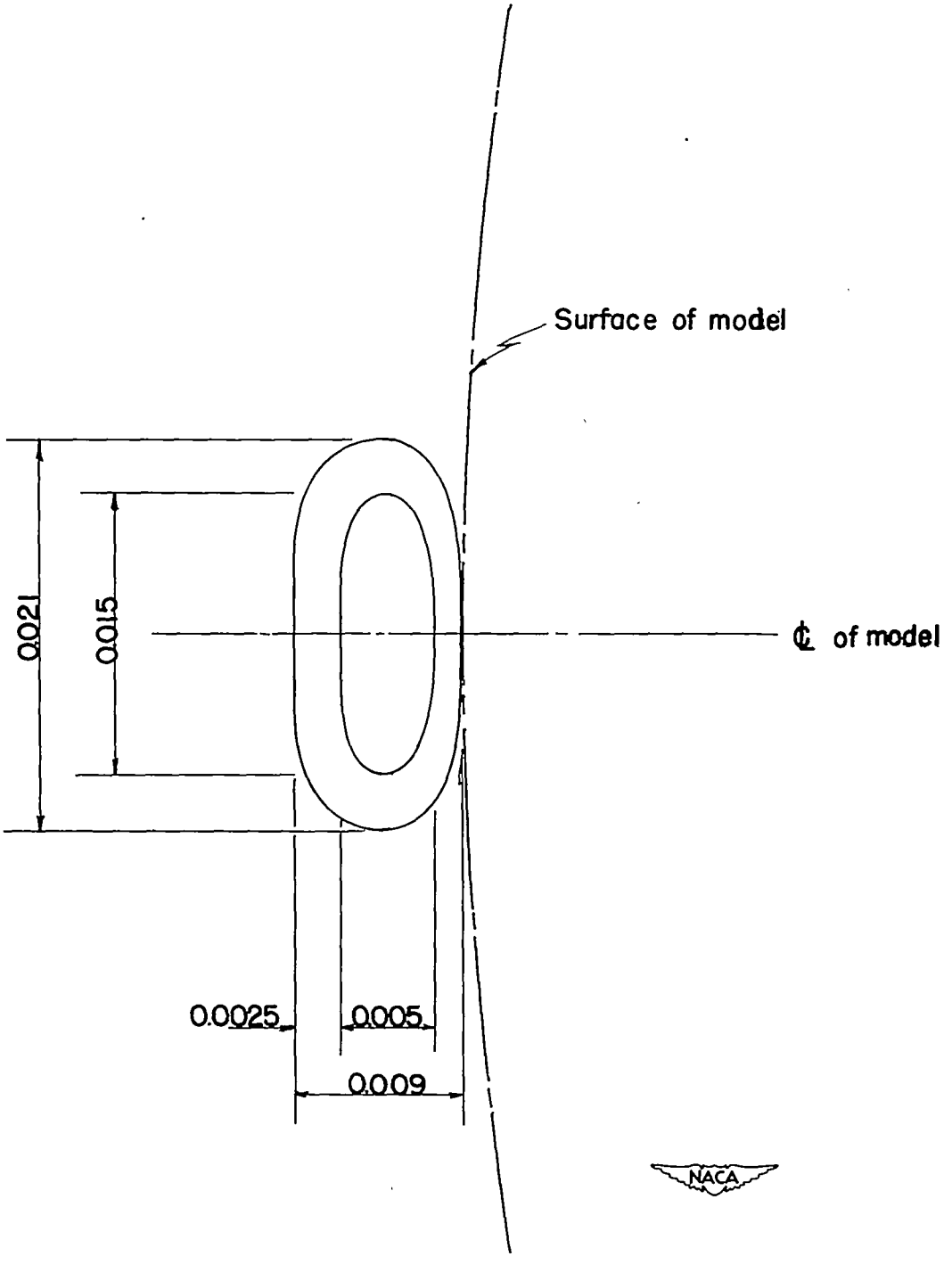

(b) Enlarged view of end of probe. Front view looking downstream
All dimensions are in inches.

Figure 2.- Concluded.

CONFIDENTIAL

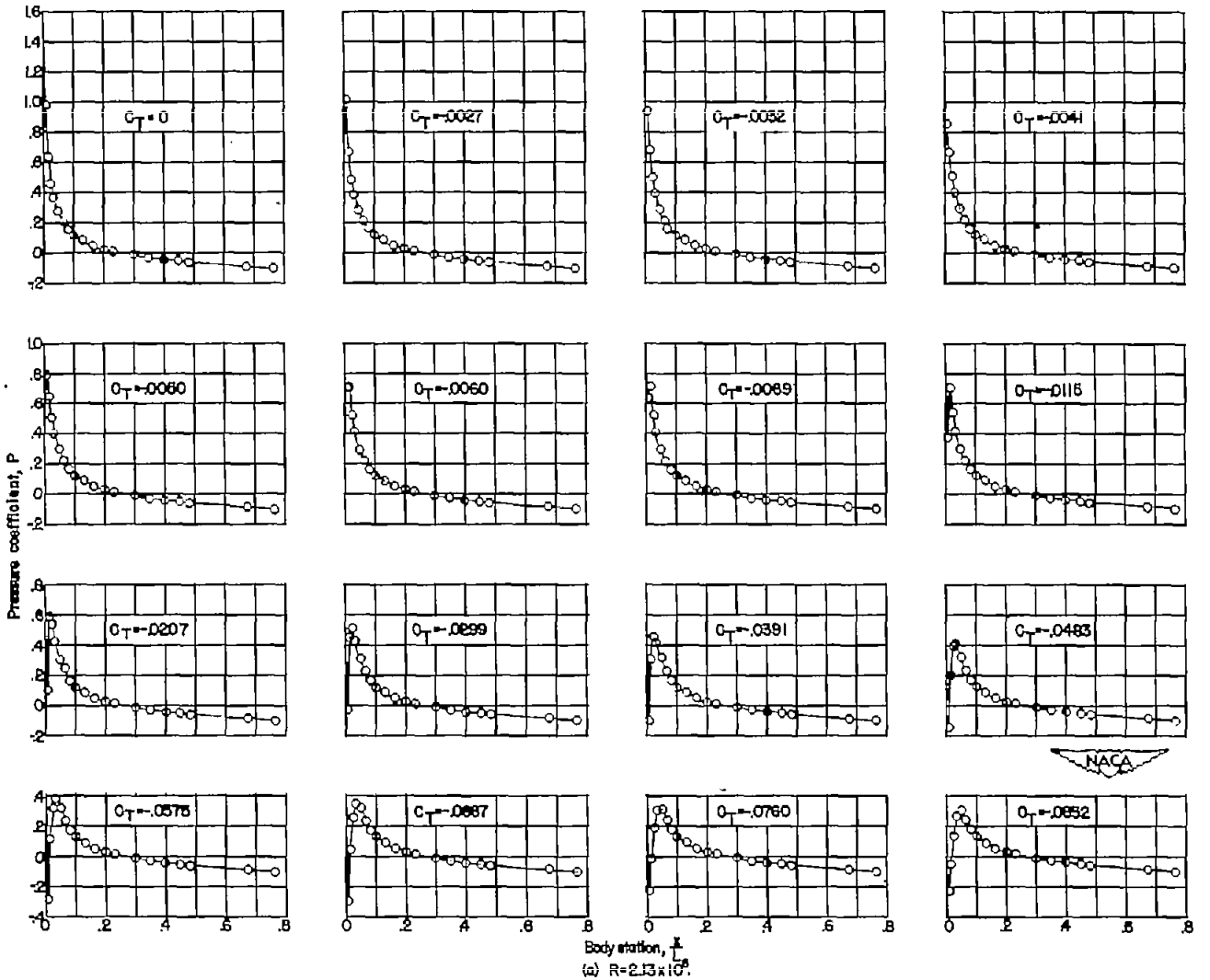

Figure 3.- Pressure distributions with varying thrust coefficient.

CONFIDENTIAL

CONFIDENTIAL

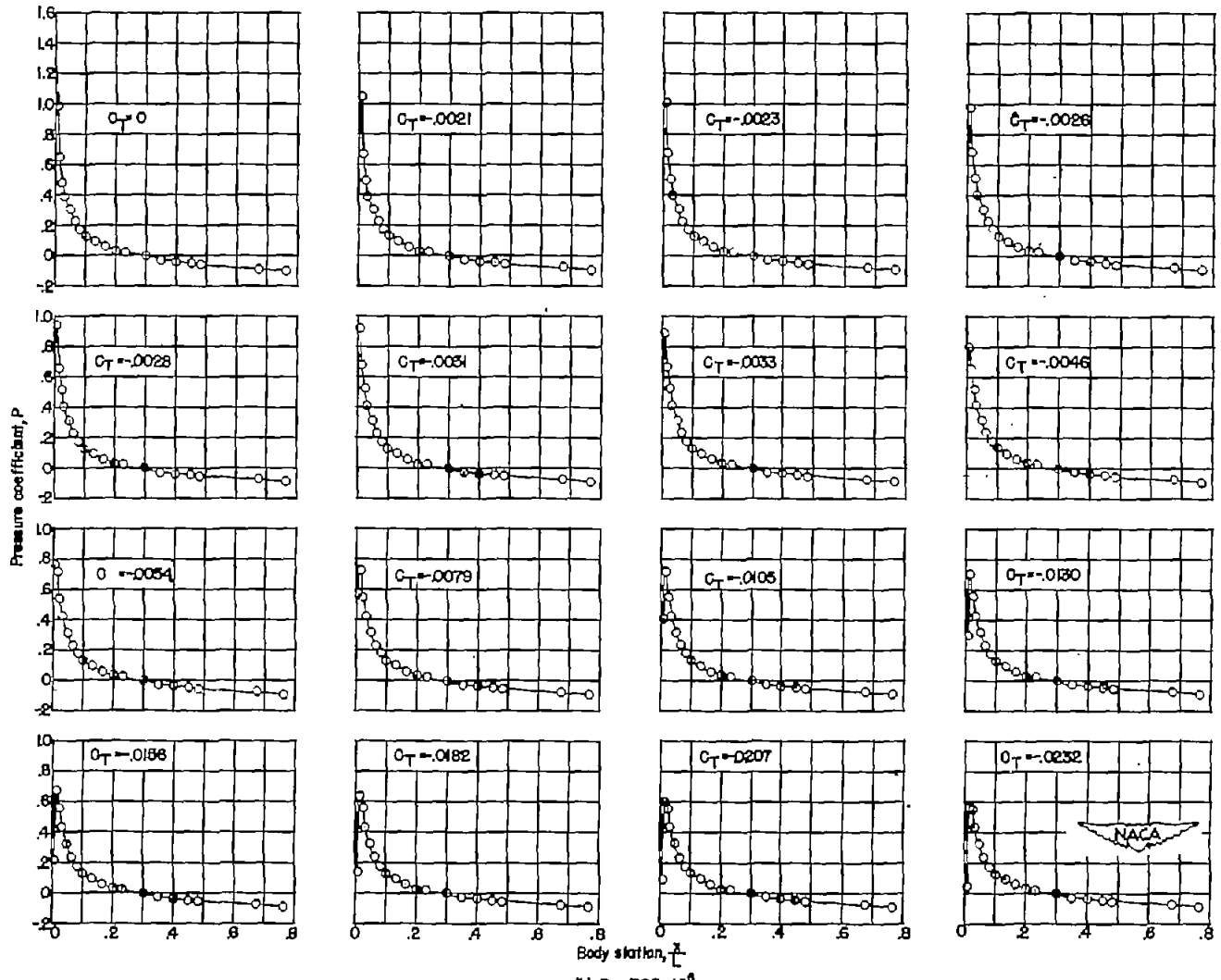

(b) $R = 7.66 \times 10^6$.

Figure 3.- Concluded.

CONFIDENTIAL

CONFIDENTIAL

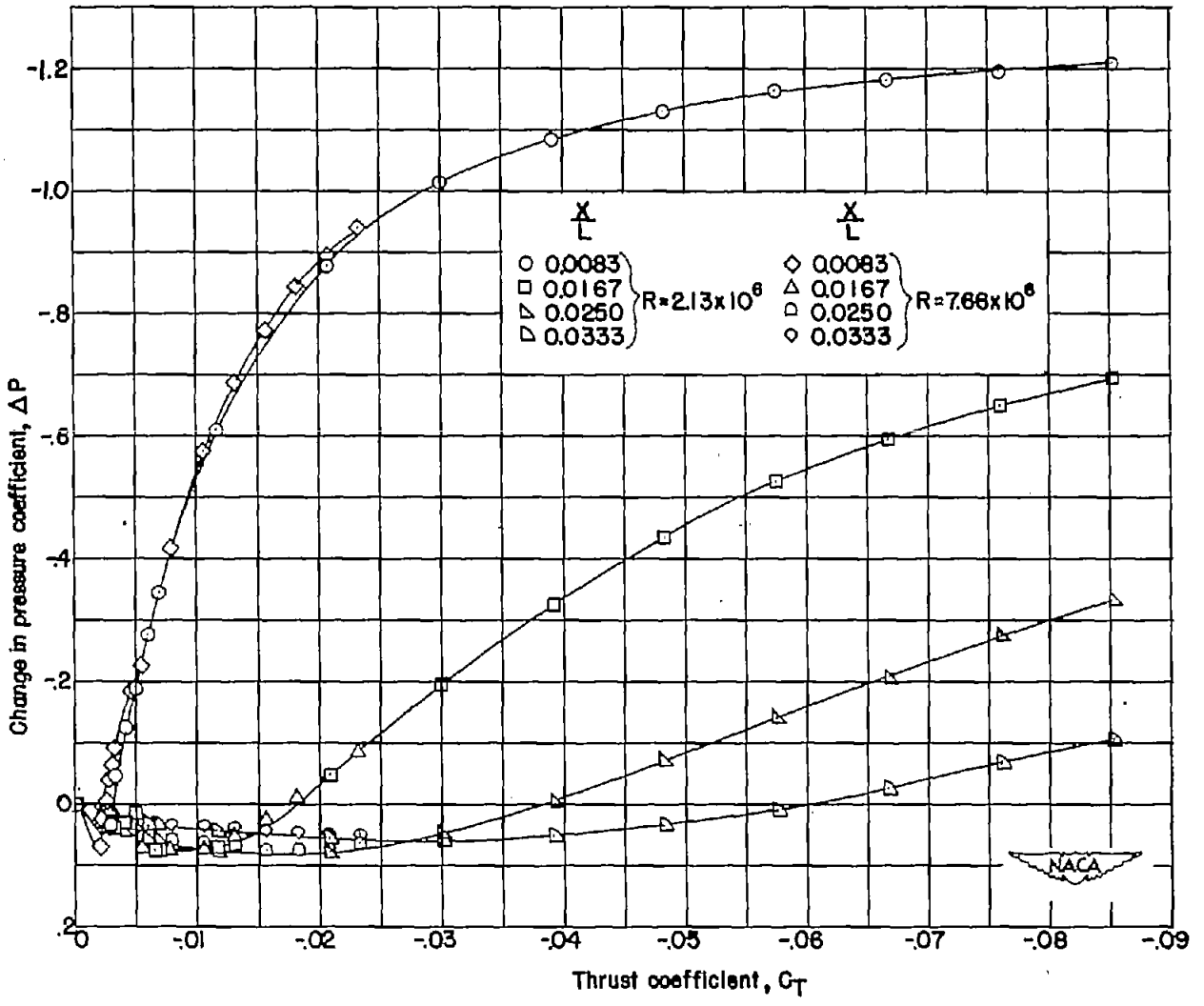

Figure 4.- Change in pressure coefficient with varying thrust coefficient for first four orifices.

CONFIDENTIAL

CONFIDENTIAL

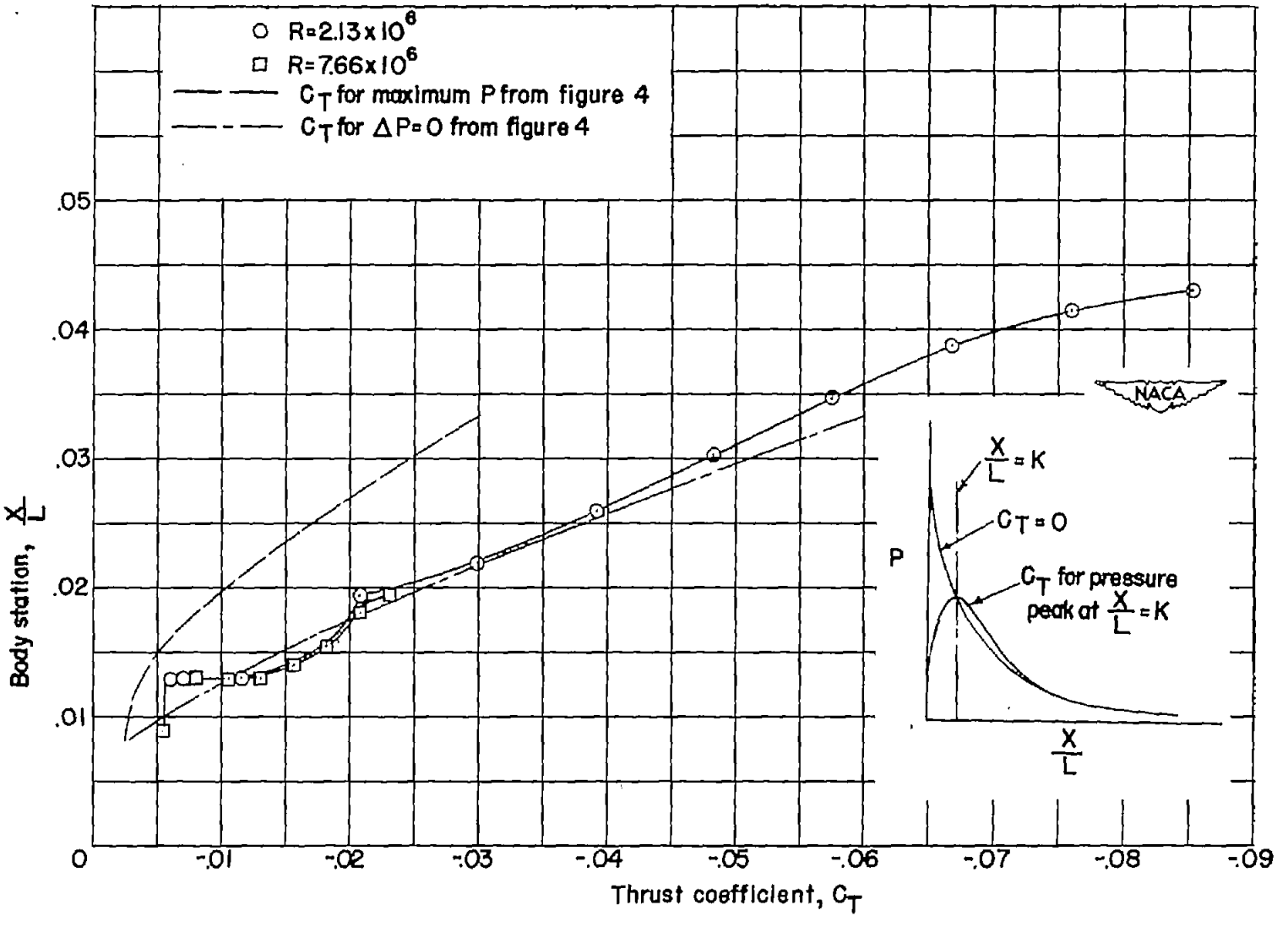

Figure 5.- Location of peak pressure with varying thrust coefficient.

CONFIDENTIAL

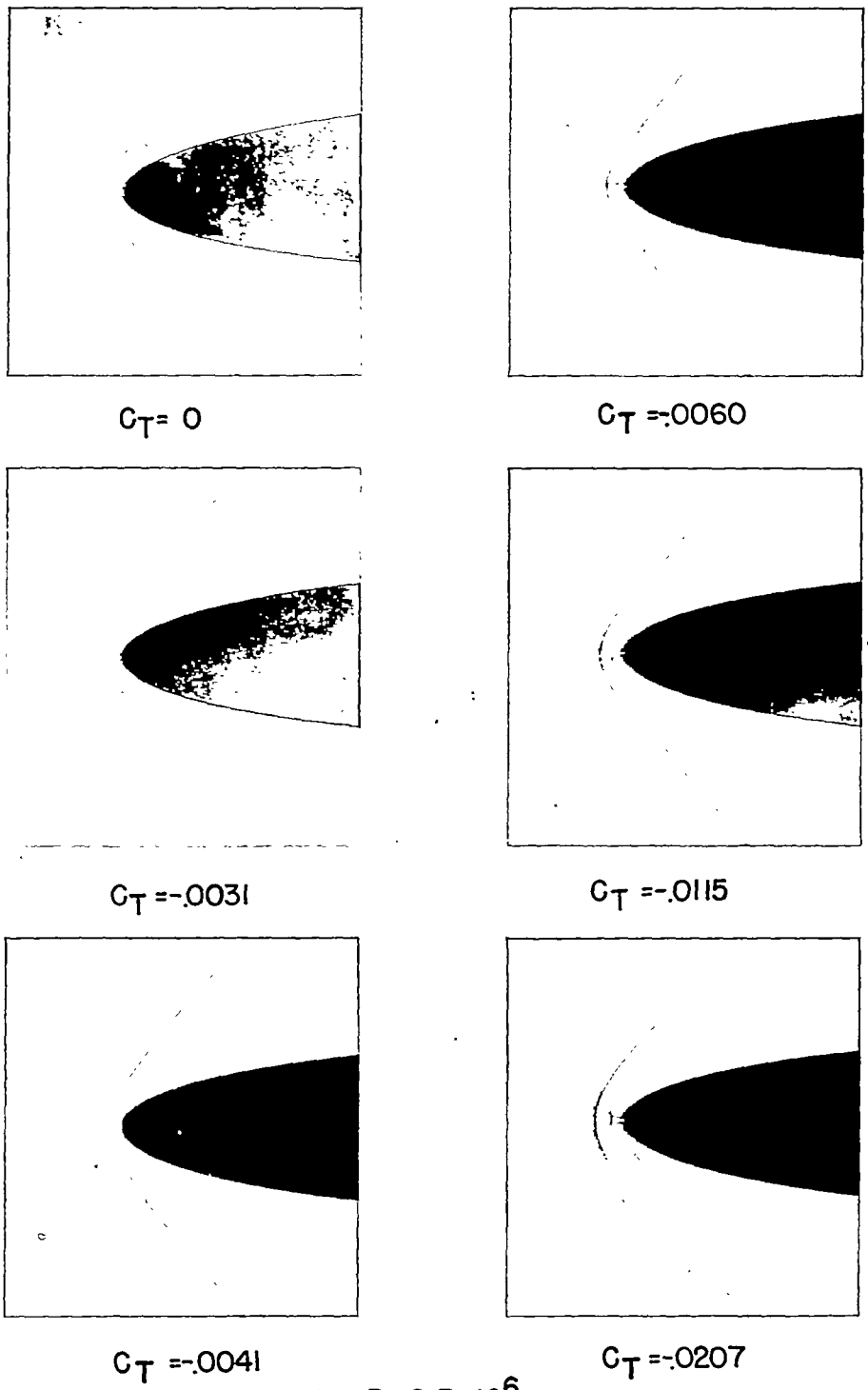

(a) $R = 2.13 \times 10^6$.

Figure 6.- Shadowgraphs of jet phenomena. L-76153

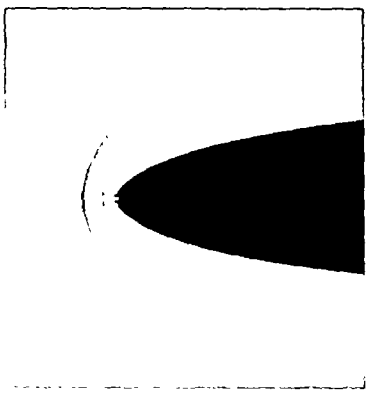

C_T =-.0299

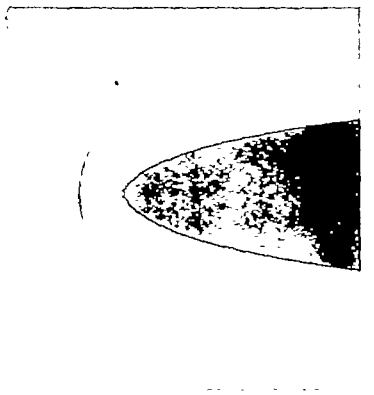

C_T =-.0575

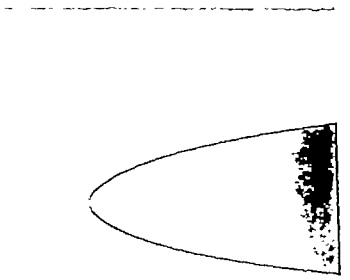

C_T =-.0390

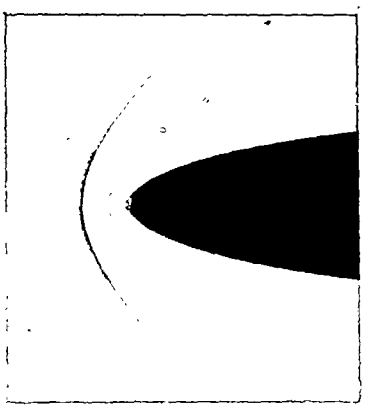

C_T =-.0666

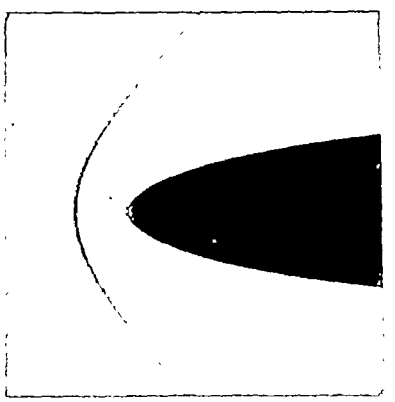

C_T=-.0852

(a) Concluded.

NACA

Figure 6.- Continued. L-76154

$C_T = 0$

$C_T = -.0028$

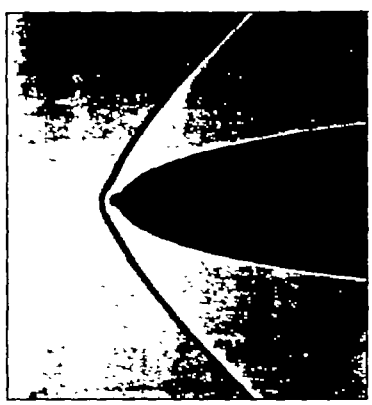

$C_T = -.0021$

$C_T = -.0044$

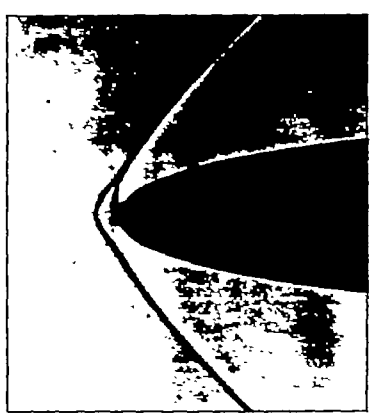

$C_T = -.0023$

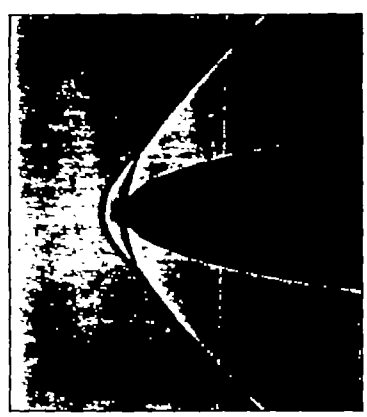

$C_T = -.0070$

(b) $R = 7.66 \times 10^6$.

Figure 6.- Continued. L-76155

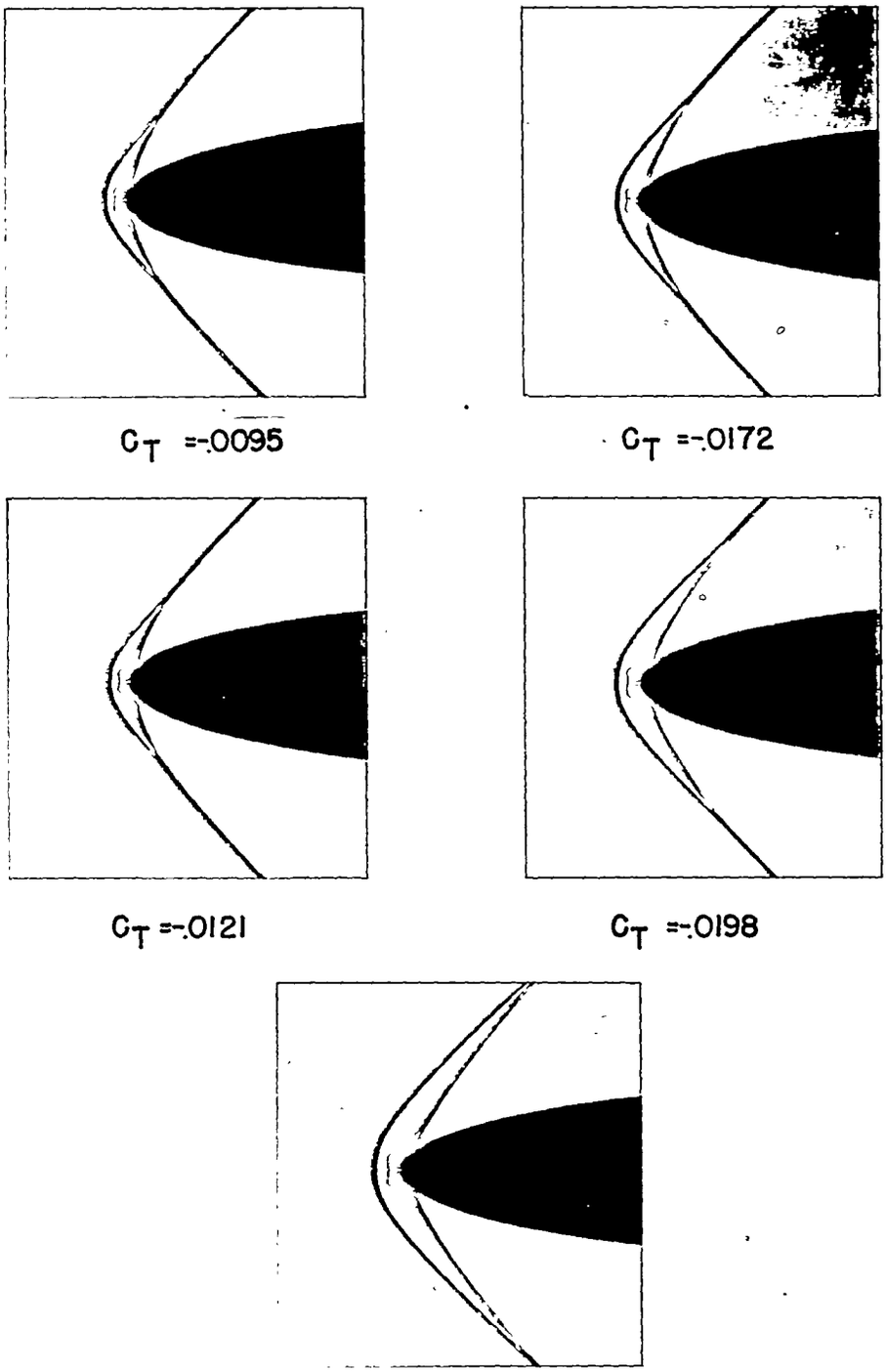

(b) Concluded.

Figure 6.- Concluded. L-76156

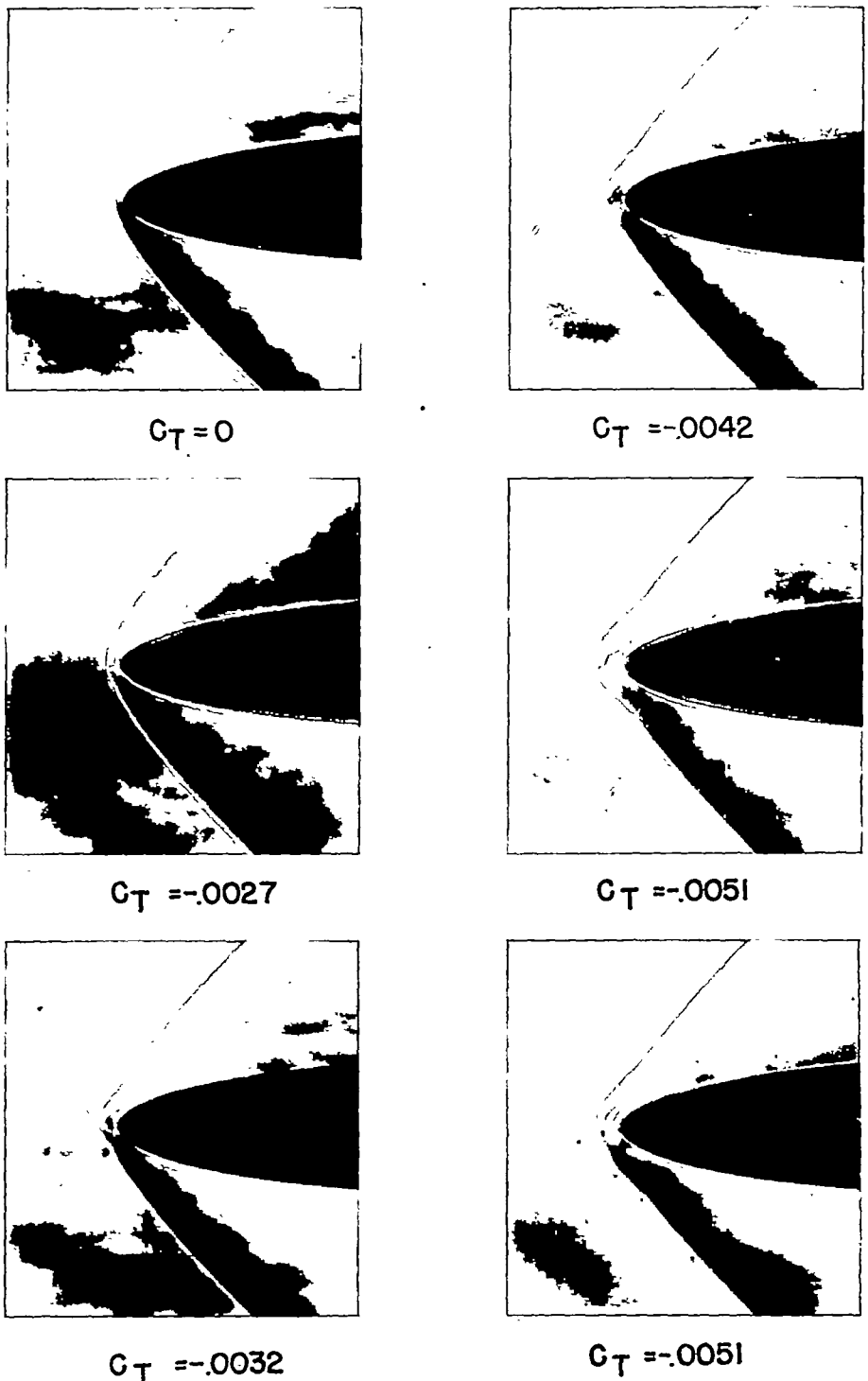

(a) $R = 2.13 \times 10^6$.

Figure 7.- Schlieren photographs of jet phenomena. L-76157

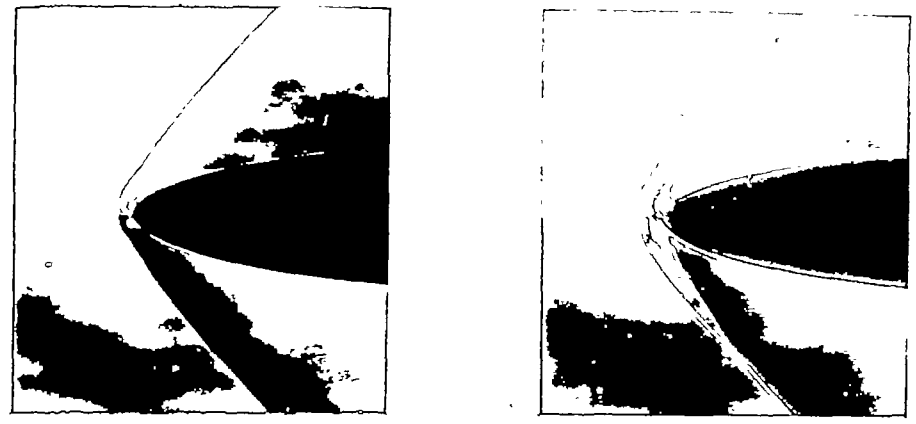

C_T =-.0060

C_T =-.0207

C_T =-.0069

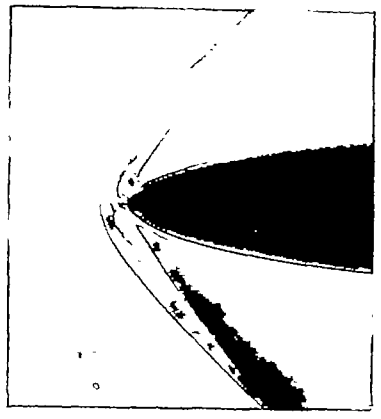

C_T =-.0299

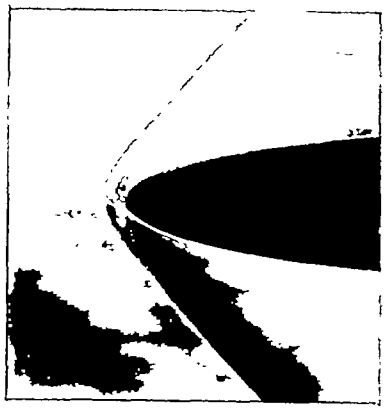

C_T =-.0115

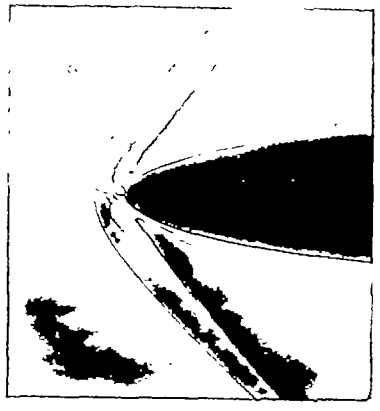

C_T =-.0390

(a) Continued.

Figure 7.- Continued. L-76158

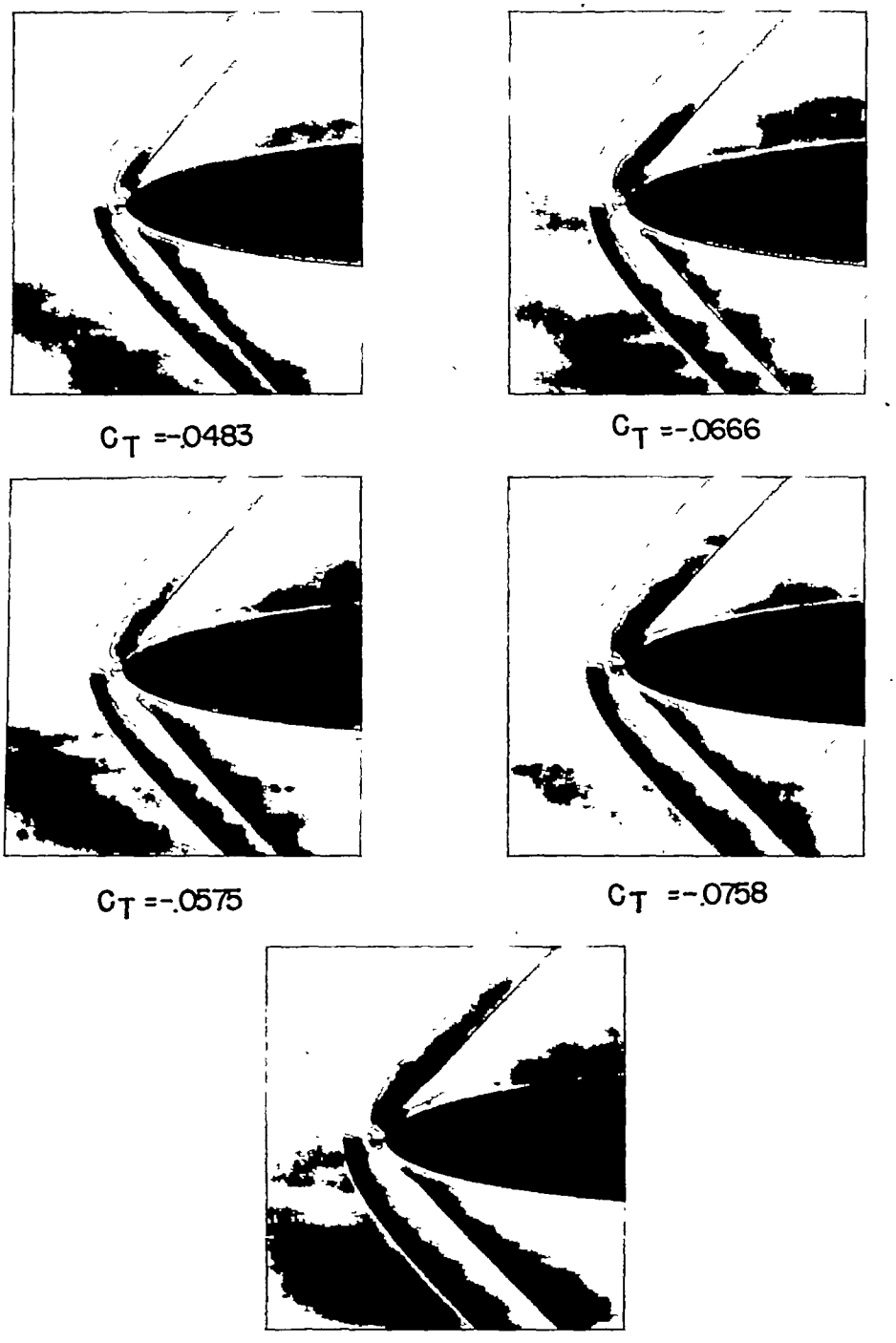

(a) Concluded.

Figure 7.- Continued. L-76159

$C_T = 0$

$C_T = -.0025$

$C_T = -.0020$

$C_T = -.0027$

$C_T = -.0022$

$C_T = -.0030$

(b) $R = 7.66 \times 10^6$.

Figure 7.- Continued. L-76161

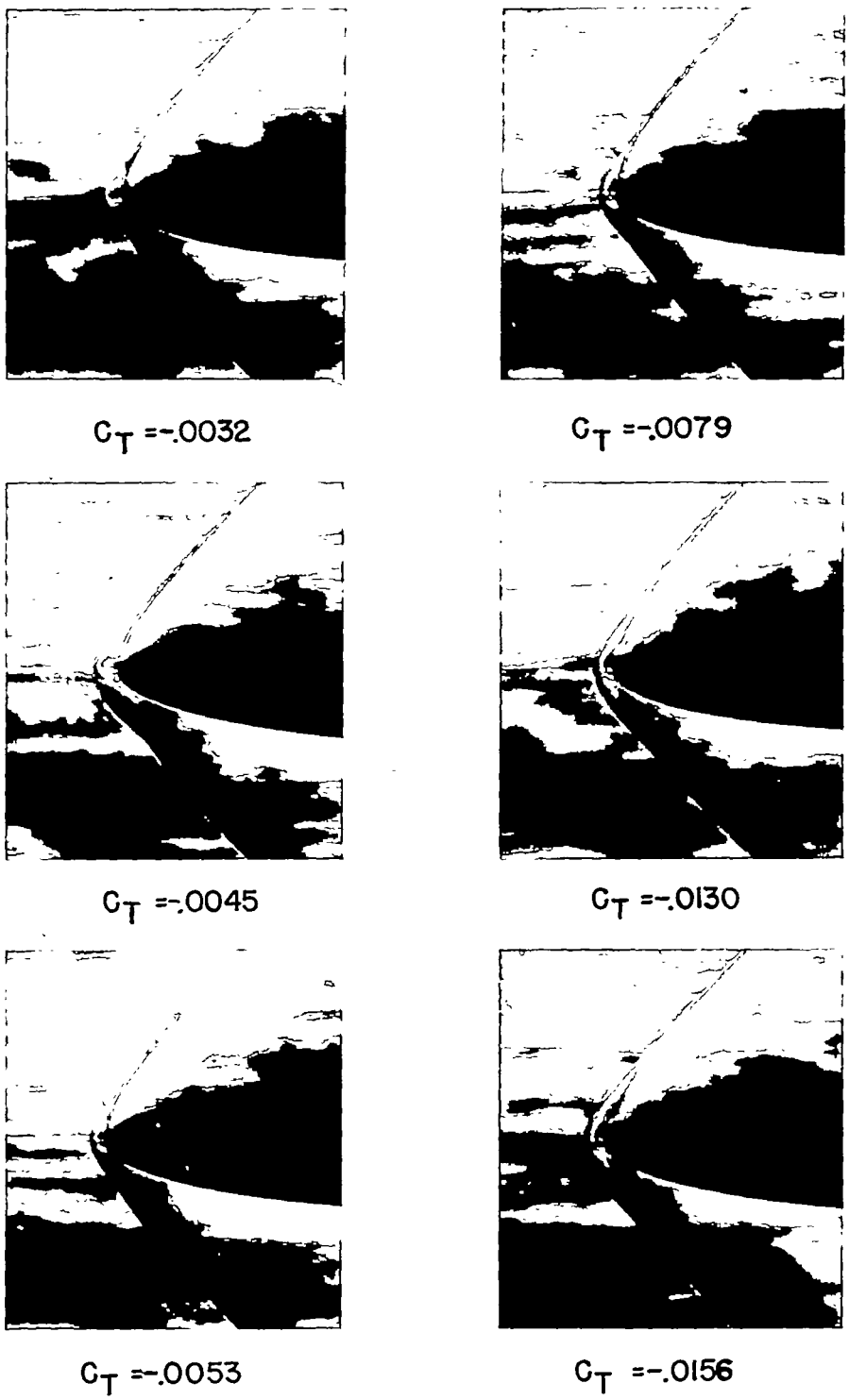

(b) Continued.

NACA

Figure 7.- Continued. L-76160

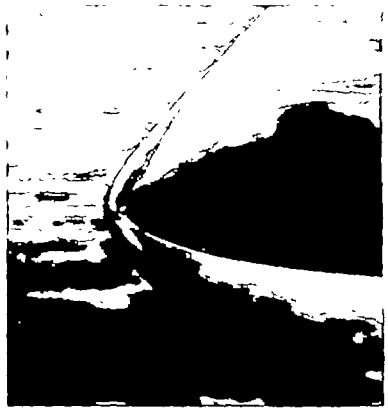

$C_T = -.0182$

$C_T = -.0207$

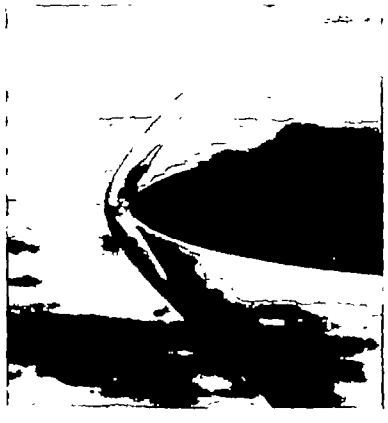

$C_T = -.0233$

(b) Concluded.

Figure 7.- Concluded. L-76162

CONFIDENTIAL

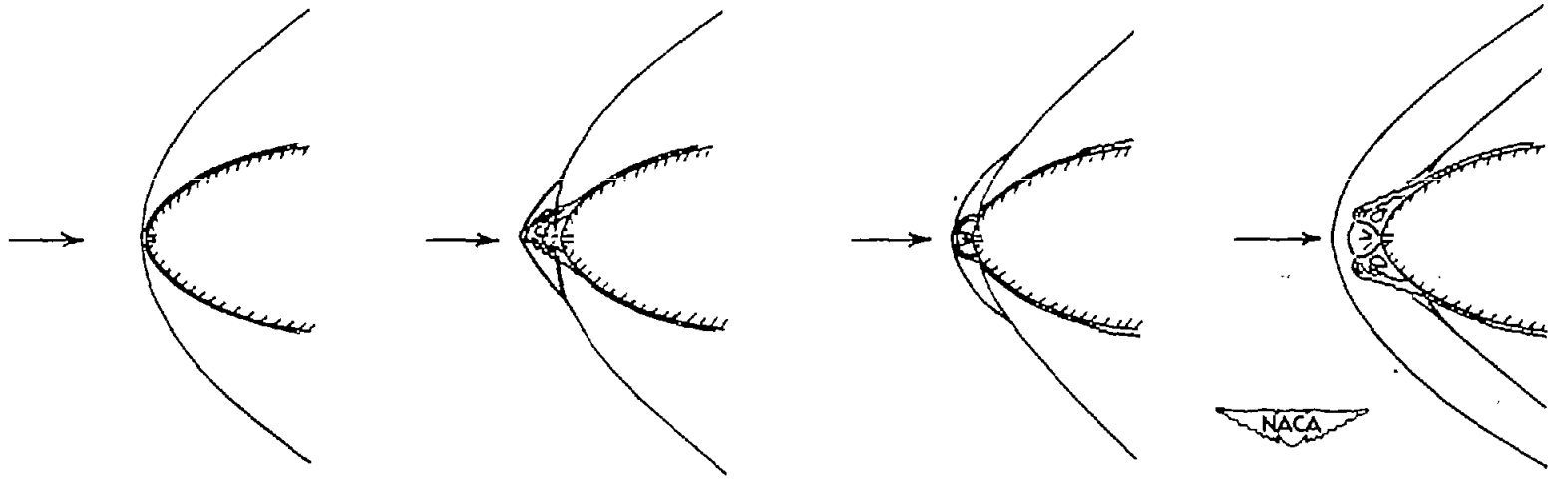

(a) $C_T = 0.$ (b) $0 > C_T > -0.0053.$ (c) $C_T = -0.0053$ to $-0.013.$ (d) $C_T \lesssim -.02.$

Figure 8.- Sketches of typical jet phenomena.

CONFIDENTIAL

CONFIDENTIAL

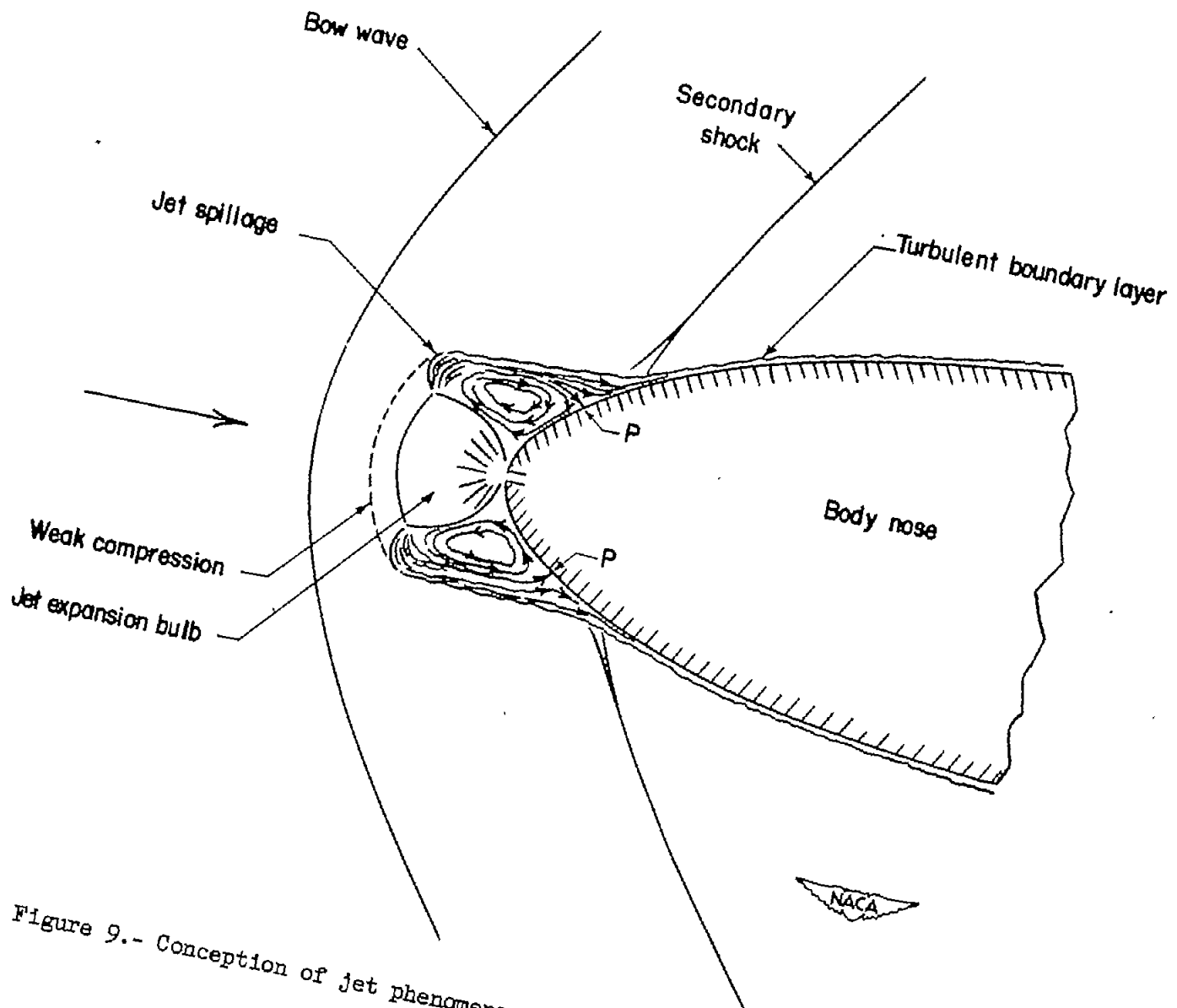

Figure 9.- Conception of jet phenomena at higher thrust coefficients.

CONFIDENTIAL

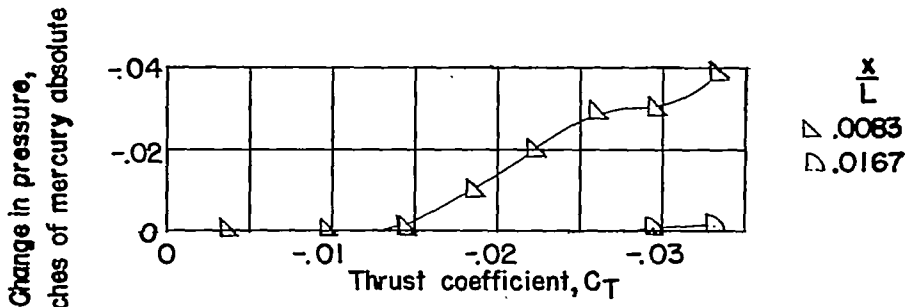

(a) Pressure variation for first two orifices.

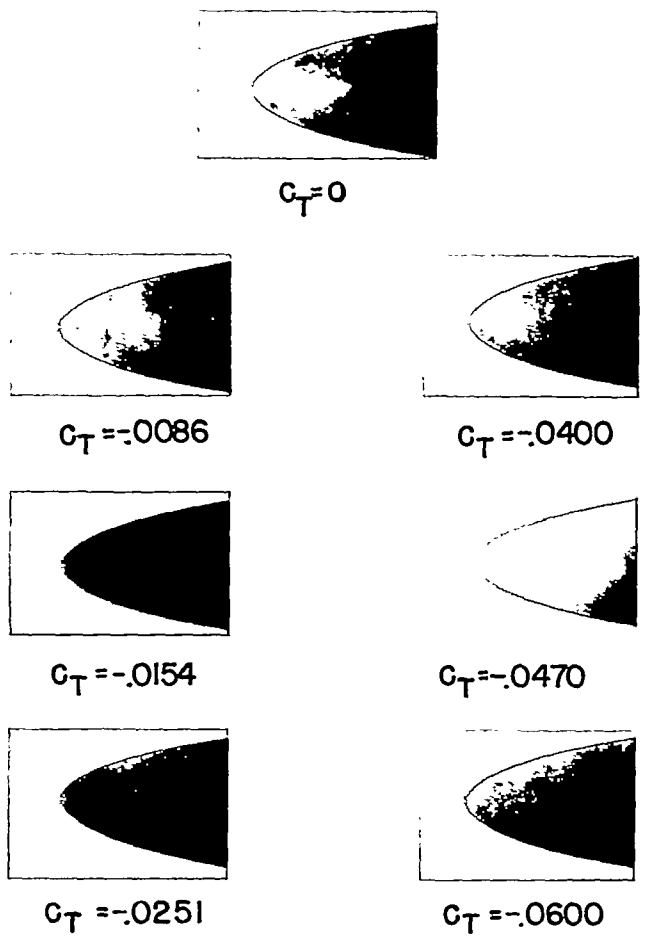

(b) Shadowgraphs of jet phenomena.

Figure 10.- Shadowgraphs and pressure effects of jet at M = 0. L-76163

CONFIDENTIAL

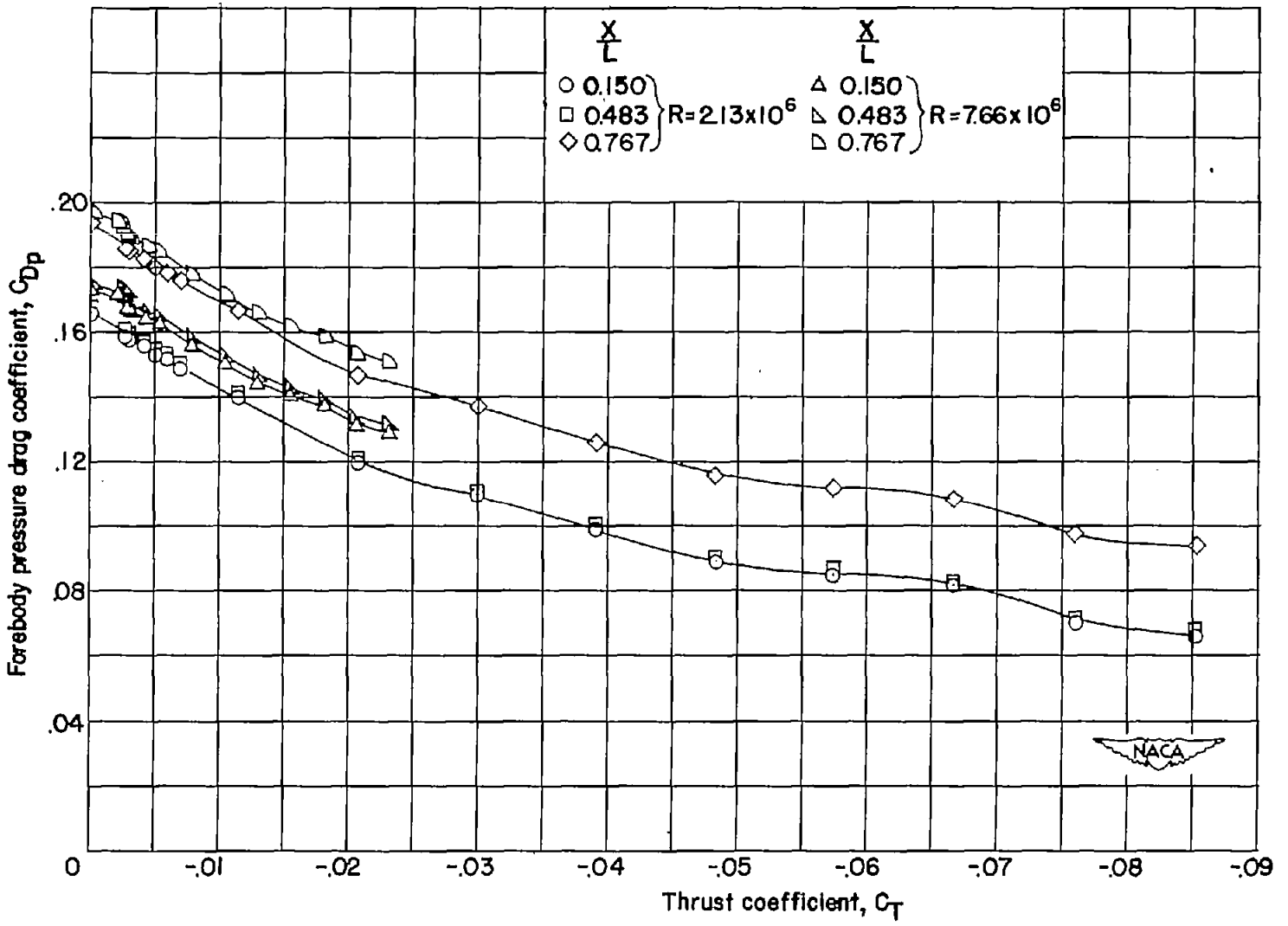

Figure 11.- Variation in forebody pressure drag coefficient with varying thrust coefficient.

CONFIDENTIAL

CONFIDENTIAL

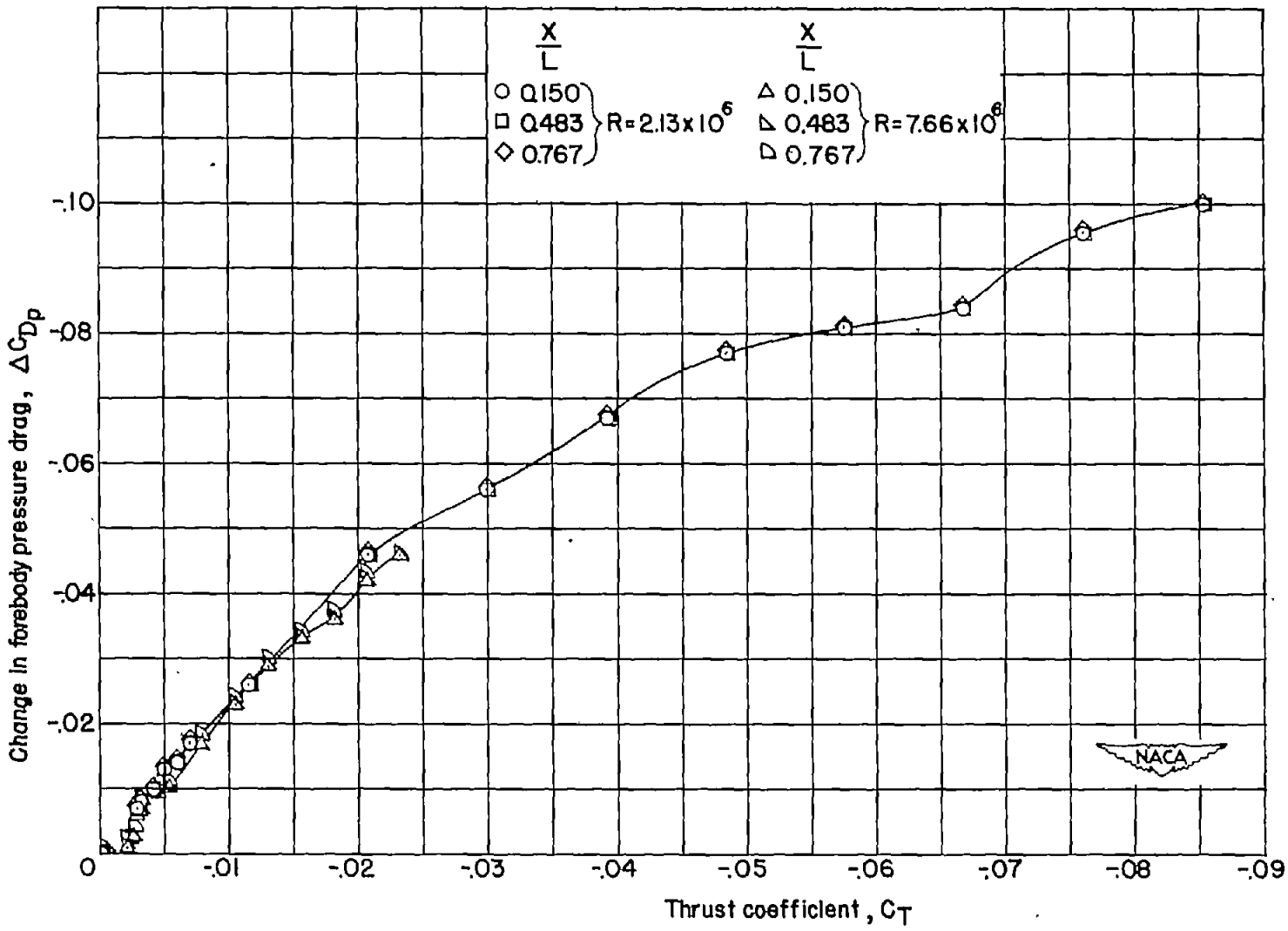

Figure 12.- Change in forebody pressure drag coefficient with varying thrust coefficient.

CONFIDENTIAL

CONFIDENTIAL

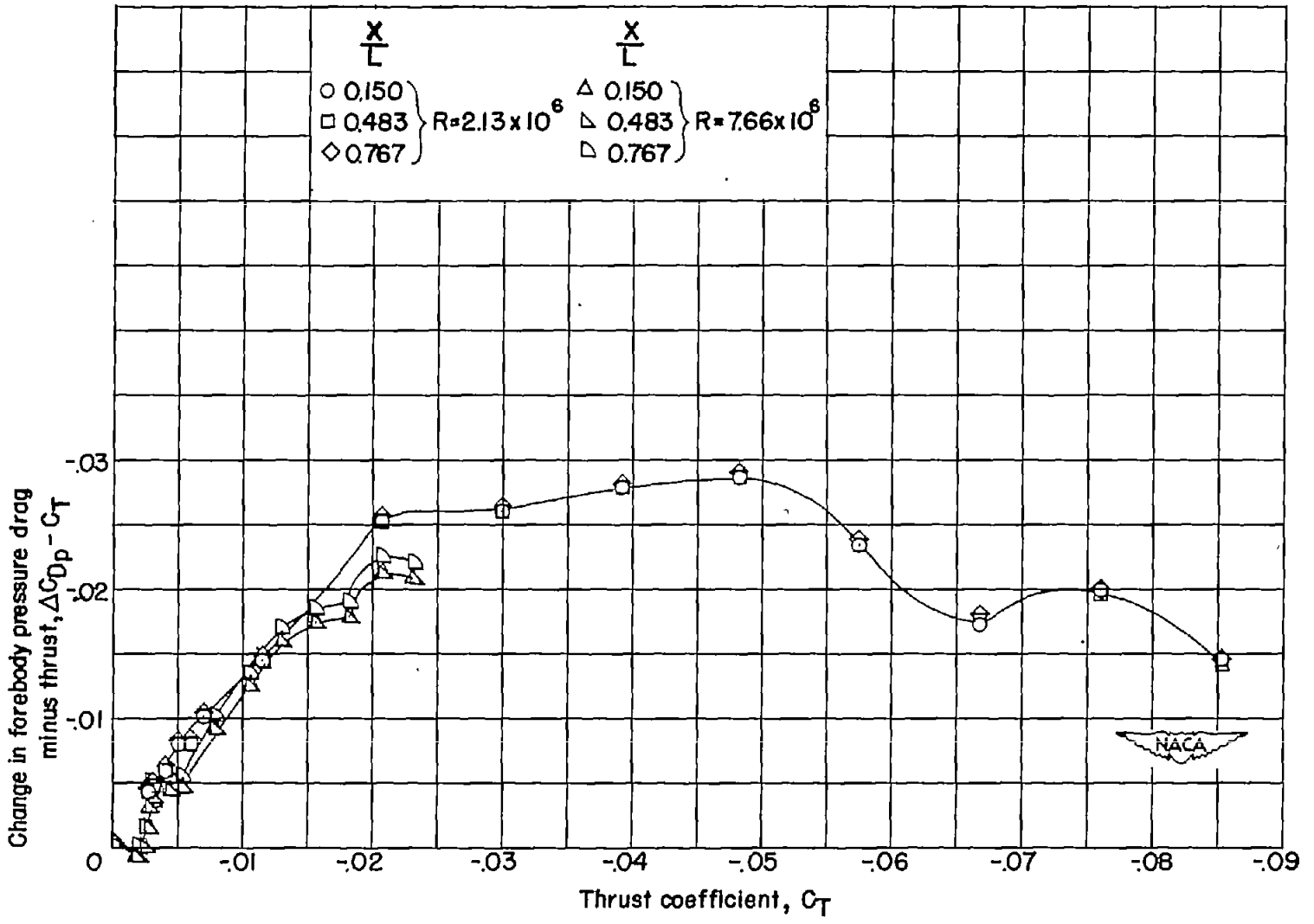

Figure 13.- Change in forebody pressure drag coefficient minus thrust coefficient with varying thrust coefficient.

CONFIDENTIAL

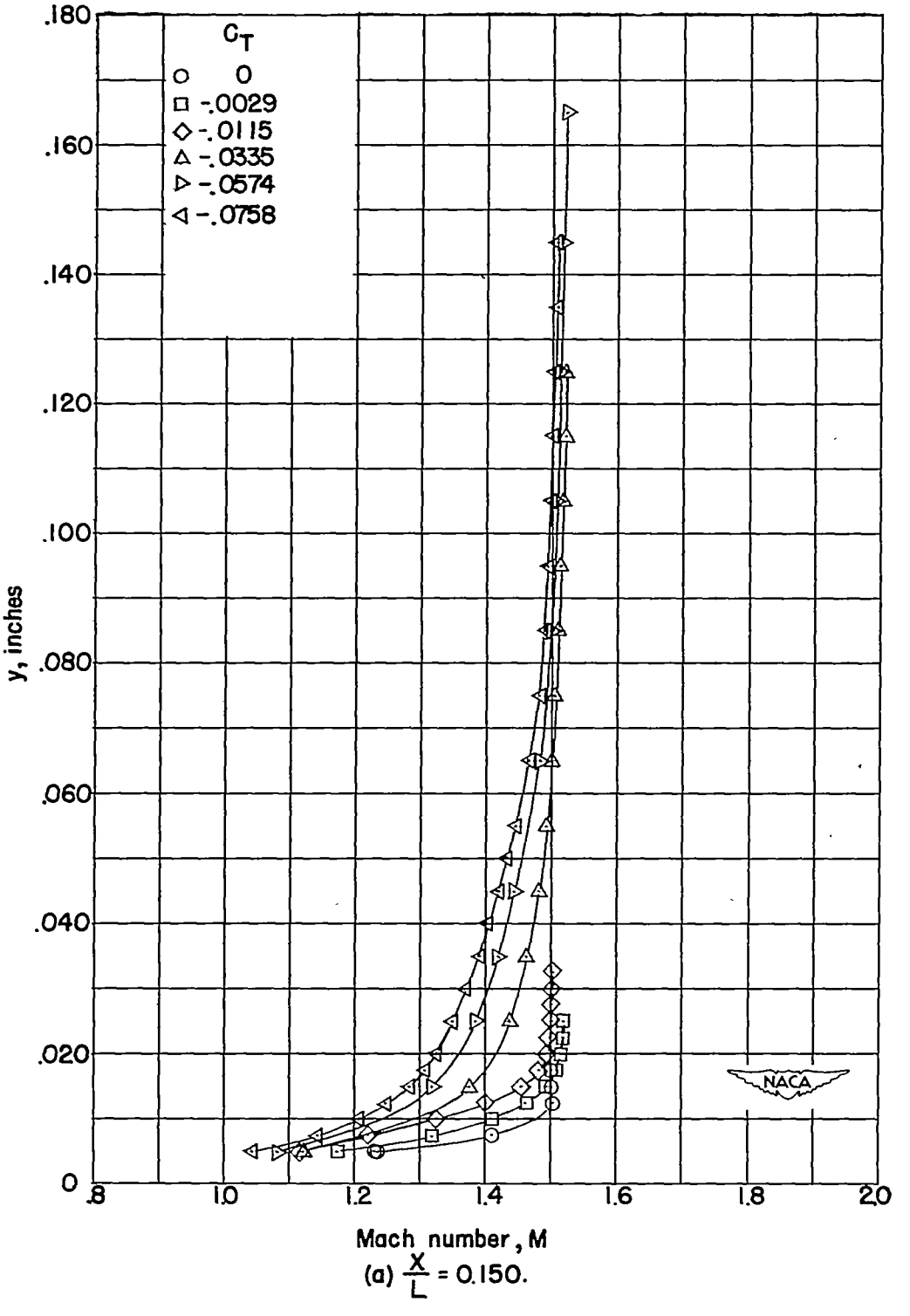

(a) $\frac{X}{L} = 0.150$.

Figure 14.- Boundary-layer profiles with varying thrust coefficient at $R = 2.13 \times 10^6$.

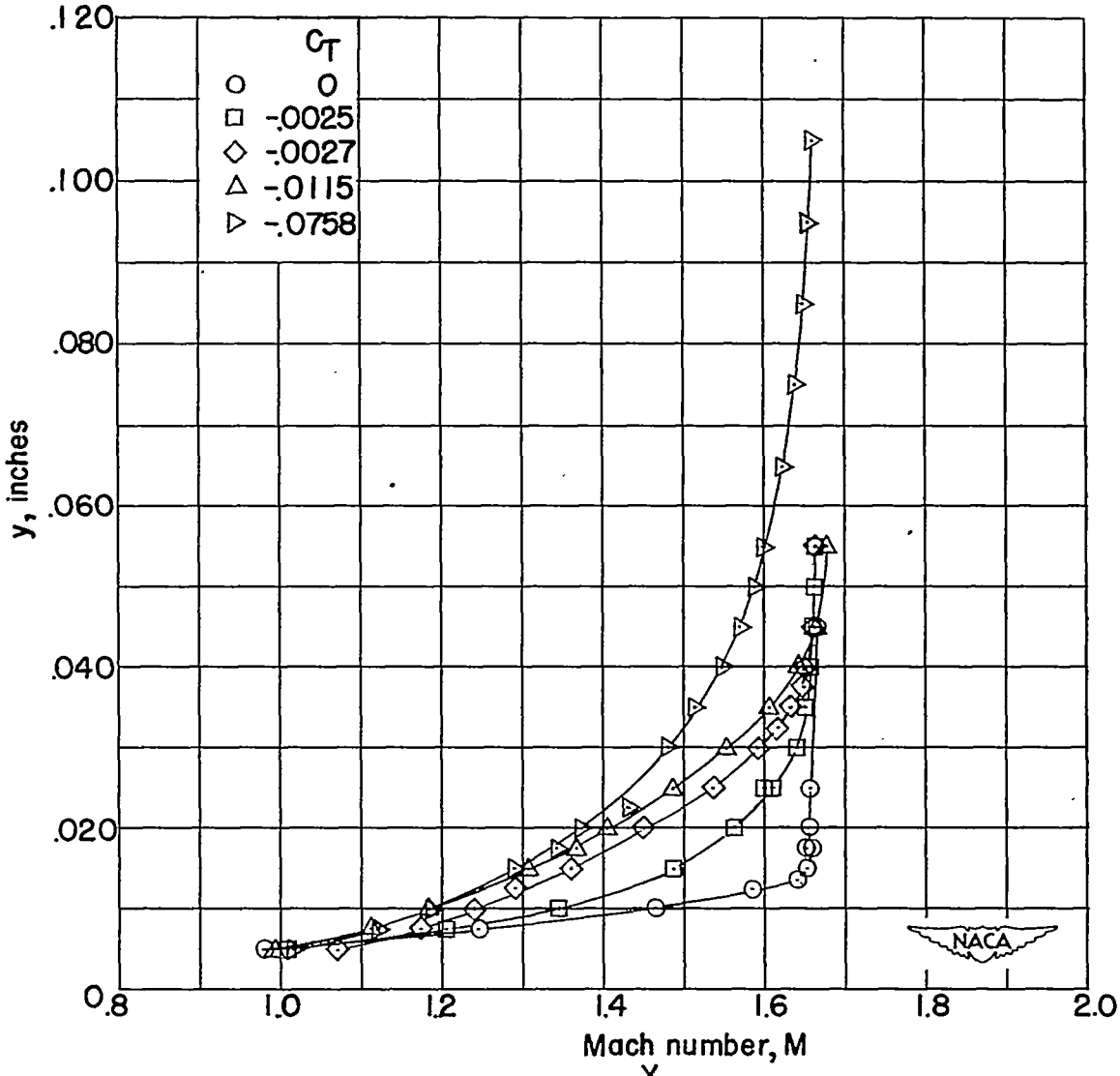

(b) $\frac{X}{L} = 0.483$.

Figure 14.- Continued.

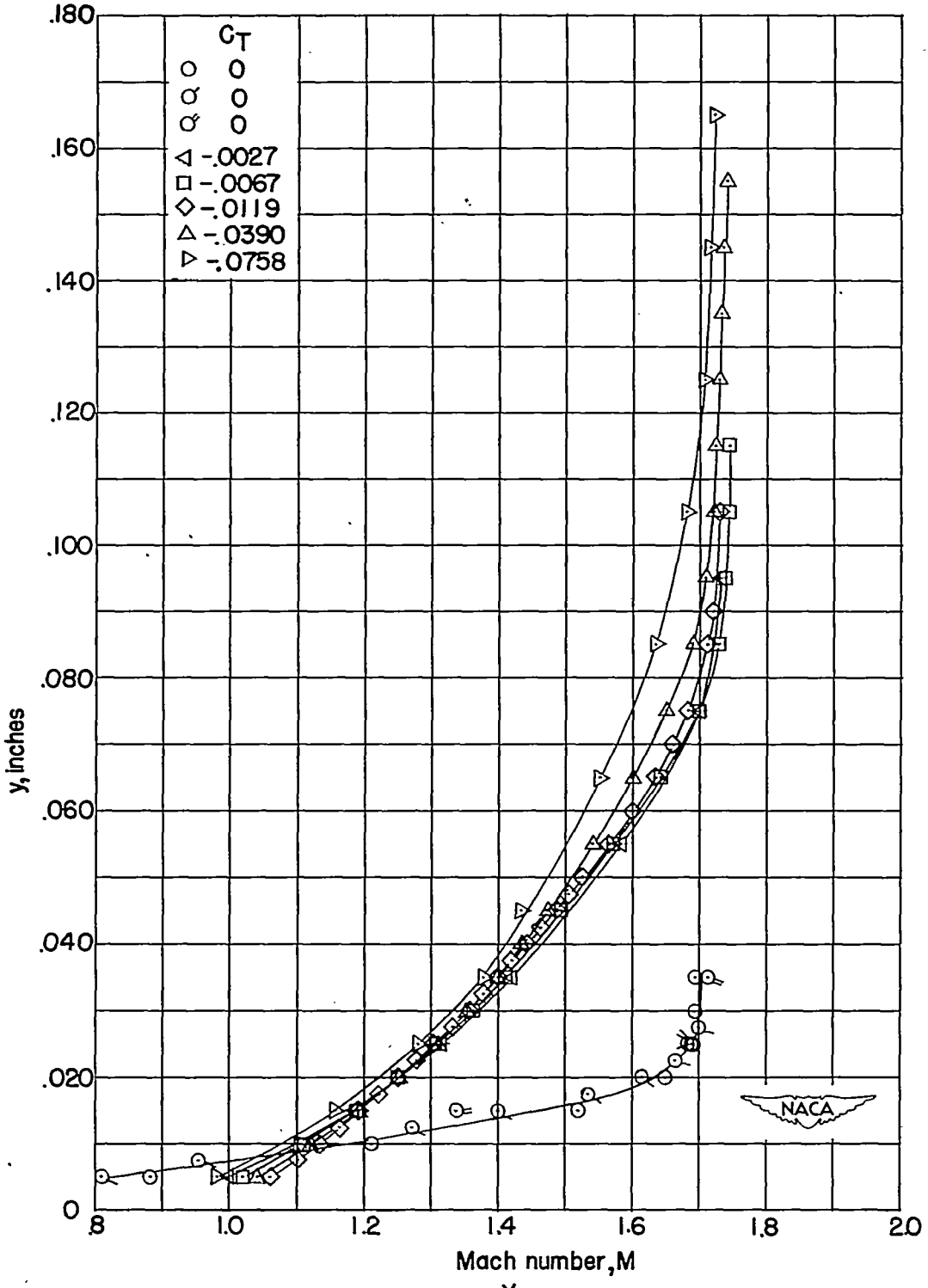

(c) $\frac{X}{L} = 0.767$.

Figure 14.- Concluded.

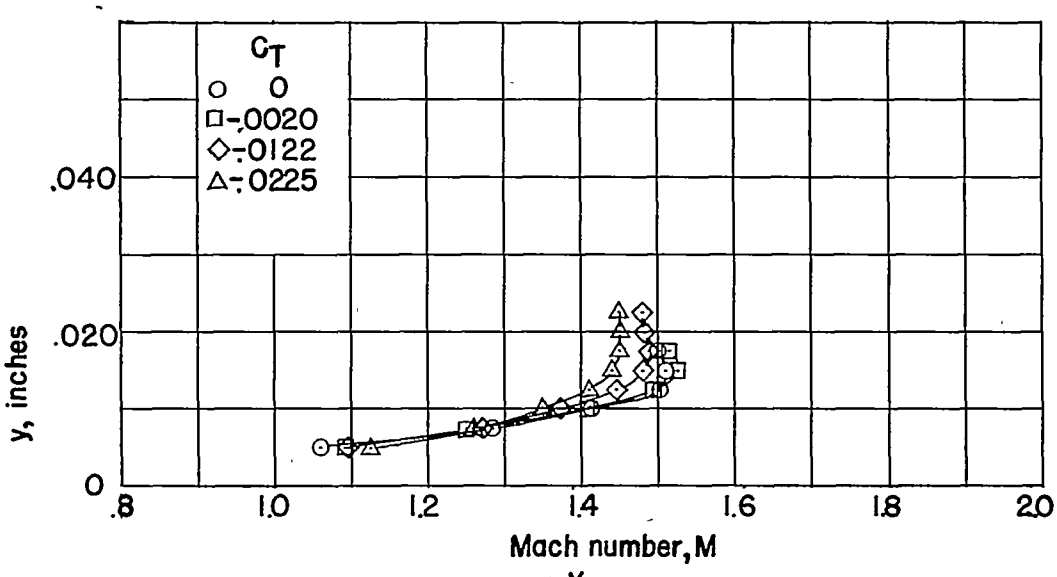

(a) $\frac{X}{L} = 0.150$.

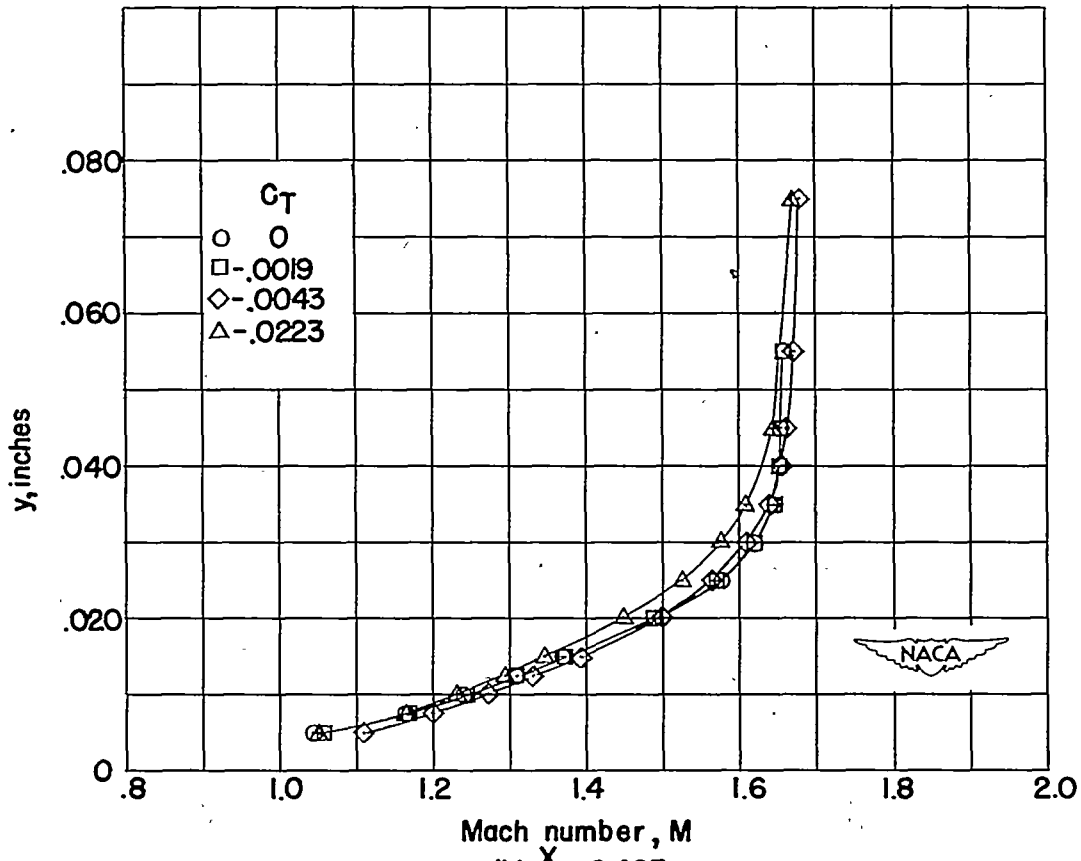

(b) $\frac{X}{L} = 0.483$.

Figure 15.- Boundary-layer profiles with varying thrust coefficient at $R = 7.66 \times 10^6$.

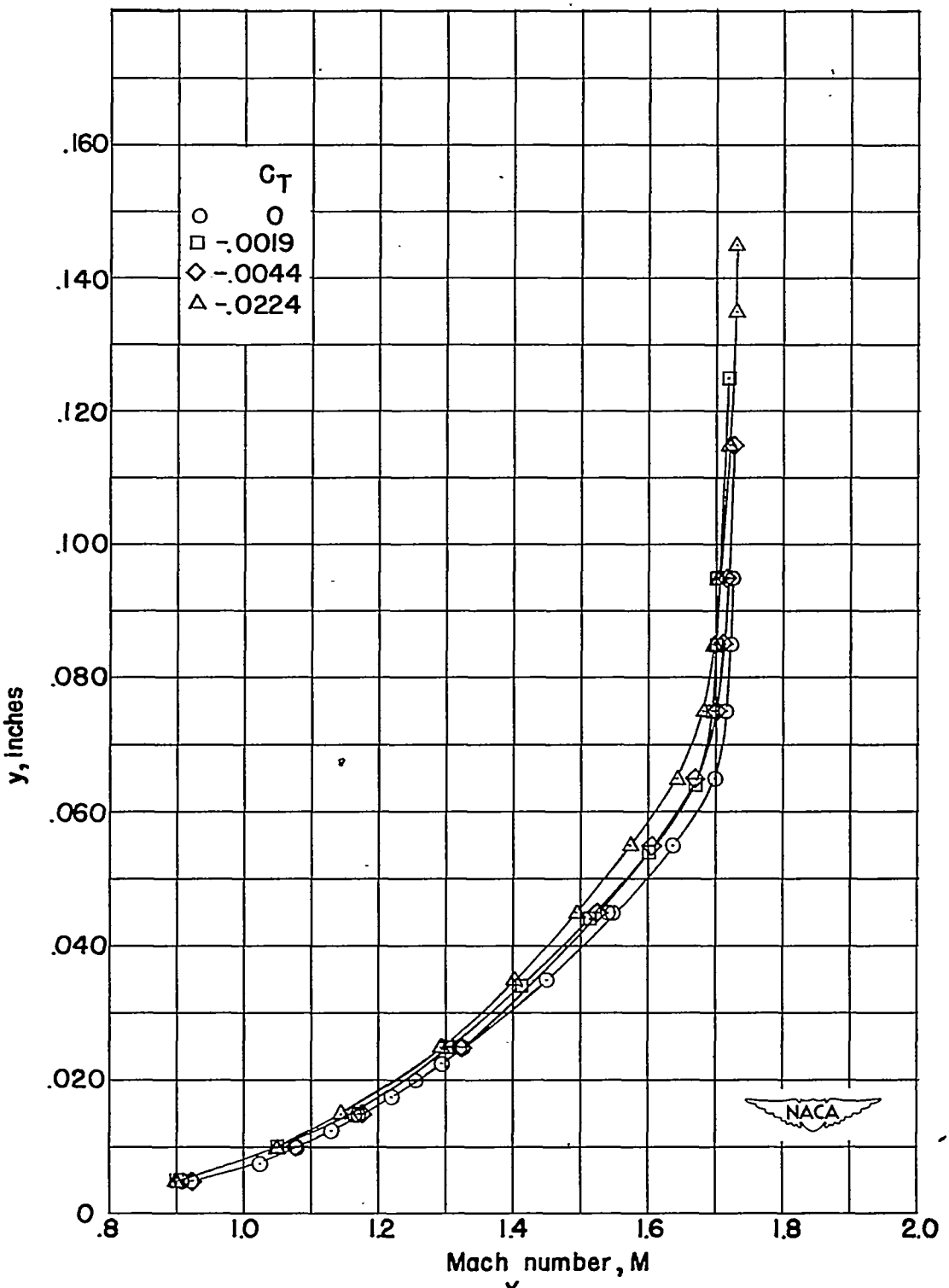

(c) $\frac{X}{L}$ = 0.767.

Figure 15.- Concluded.

CONFIDENTIAL

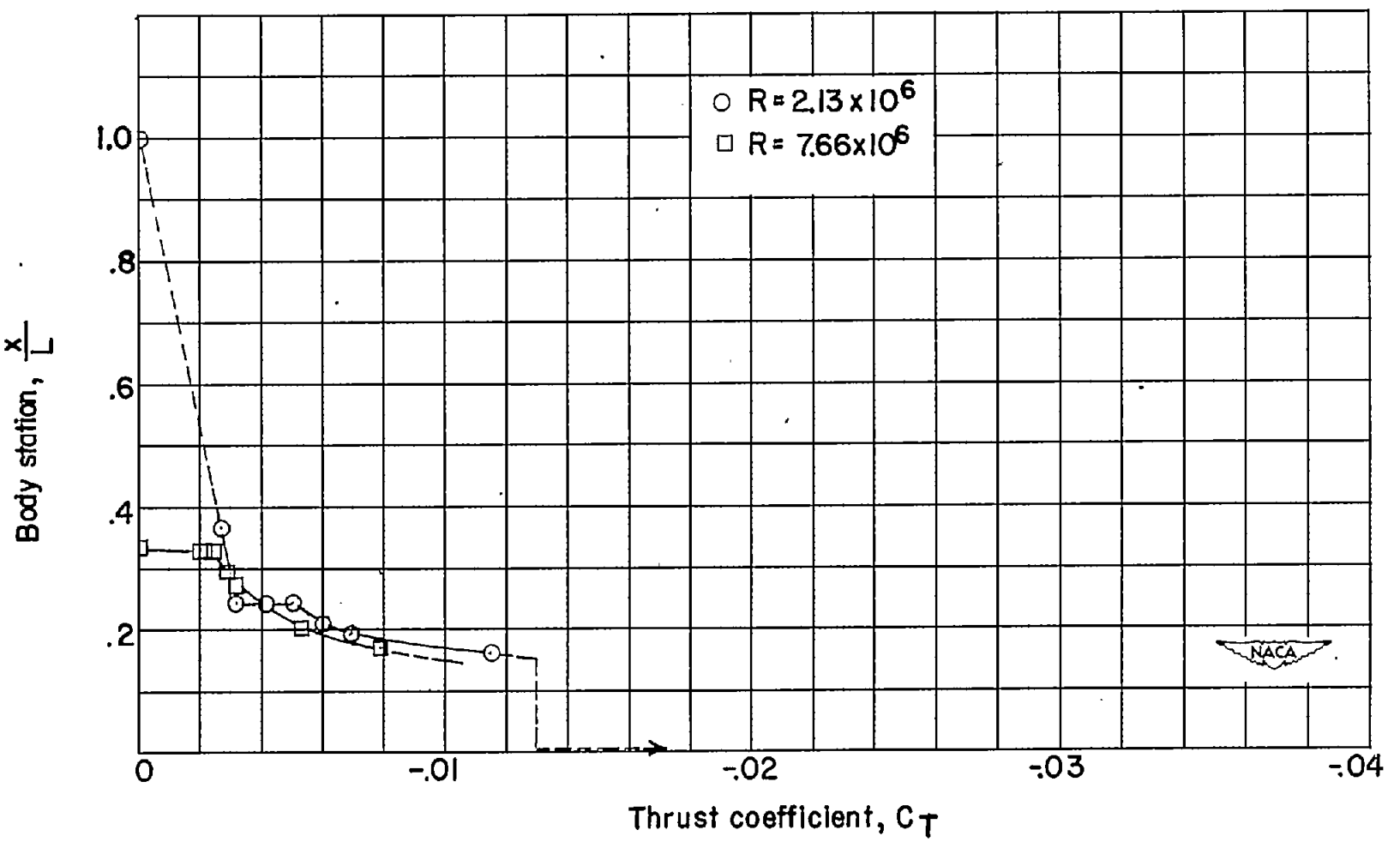

Figure 16.- Change in location of transition point on body surface with varying thrust coefficient.

CONFIDENTIAL

NACA-Langley - 11-13-52 - 350